Charles University
Faculty of Science

Study program:
Geology

M.Sc. Jaime Yesid Suarez-Ibarra

PALAEOCEANOGRAPHIC EVOLUTION OF THE WESTERN SOUTH ATLANTIC DURING MARINE ISOTOPE STAGES 5 – 1: A FORAMINIFERAL PERSPECTIVE

Doctoral thesis

Supervisor:
prof. RNDr. Katarína Holcová, CSc.

Advisors:
Ph.D. Thibault de Garidel-Thoron
Dr. rer. nat. Manuel F.G. Weinkauf

Prague, 2024

Declaration of honour

I hereby declare that this Ph.D. thesis was written by me and exclusively with the literature listed in the References.

In Prague, 09. 09. 2024.

Abstract

This cumulative thesis reconstructs past changes in surface primary productivity and carbonate dissolution in the western South Atlantic Ocean, particularly the southernmost Brazilian continental margin, focusing on the Marine Isotope Stages 5 – 1. Comprising two published articles, one submitted manuscript, and this integrative text, this PhD thesis aims to contribute to our understanding of the mechanisms behind such variations and the dynamics of this area during the past interglacial-glacial cycle, as well as its potential role in carbon cycle processes.

The first article explores surface palaeoproductivity and benthic environmental conditions by analysing the sediment core SAT-048A, spanning 5 – 43 ka, from the continental slope of the southernmost Brazilian continental margin. Using micropalaeontological, geochemical, and sedimentological data, the study identifies a positive correlation between palaeoproductivity proxies and carbonate dissolution. It demonstrates that higher productivity and organic matter flux during glacial periods led to increased dissolution rates of planktonic foraminifera tests, driven primarily by productivity rather than by changes in the Atlantic Meridional Overturning Circulation.

The second manuscript examines the last interglacial-glacial cycle using core SIS-249, spanning 30 – 110 ka, also recovered from the continental slope of the southernmost Brazilian continental margin. It reconstructs past changes in sea surface productivity, stratification, and carbonate dissolution, suggesting a ~43 kyr cycle, likely related to the obliquity cycle. Enhanced productivity is attributed to glacial upwelling (due to a reduced stratification) of nutrient-rich waters and obliquity-paced continental fertilisation. The study highlights the role of organic matter bioavailability in driving calcium carbonate dissolution and suggests potential influences of corrosive Southern Component Water.

The submitted manuscript quantifies ecological and taphonomical signals in the test size variation of planktonic foraminifera from core SAT-048A. Notably, smaller sizes during periods of enhanced surface productivity, which is consequent with elevated carbonate dissolution. It provides a framework to understand the differential effect of dissolution on calcite tests which without proper identification can lead to

underestimation of test sizes (by ~25±9%) and planktonic foraminifera fragmentation, potentially impacting foraminifera-based ecology and geochemical proxies.

The integrative text of this PhD thesis synthesises the abovementioned articles and manuscript, further discussing them in a global context, highlighting the strong connection between Antarctic system's dynamics and the southern hemisphere, as well as how they may respond to orbital cycles and regulate atmospheric CO_2 levels. Chapter 5 presents a detailed study on core SIS-203, discussing calcium carbonate dissolution over the 7 – 31 ka interval, which is planned to be submitted. This chapter investigates carbonate production, dilution, dissolution, and bottom current processes. Aided by new εNd analyses in foraminiferal coatings, it suggests a strong relationship between dissolution and changes in bottom water mass geometry at mid and deep waters. Altogether, this thesis suggests that past changes of carbonate dissolution in the study area are similar to modern patterns in the oceans, being related to metabolic CO_2 release in shallow waters and calcite solubility at greater depths.

This study highlighted some key gaps in our knowledge of the palaeoceanography of the western South Atlantic, and therefore future research should investigate more complete and longer temporal records in the southwestern Atlantic to fully understand the influence of orbital parameters and Antarctic's dynamics on biogeochemical processes (i.e., continental fertilisation due to enhanced southwesterly winds), exploring the role of the study area in global carbon cycling.

Table of Contents

Chapter 1:
Introduction

The atmospheric carbon-dioxide concentration (pCO_2) is tightly related to the biospheric, geological and climatic systems[1]. Palaeoclimatic studies have documented pCO_2 fluctuations during the Quaternary glacial-interglacial stages before the industrial revolution, with concentrations remaining below 400 ppm over the past two million years[2–4]. However, anthropogenic CO_2 emissions have resulted in an unprecedented increase of the pCO_2 over the last 250 years, leading pCO_2 to exceeding 400 ppm[5]. This rise in CO_2 emissions contributes to increasing the greenhouse effect, trapping more heat and leading to global warming. Additionally, CO_2 dissolves in seawater forming carbonic acid, lowering the ocean's pH and causing ocean acidification[6]. These processes destabilise the climate system[7], occasioning far-reaching changes in natural ecosystems[8–11] and a current climatic crisis affecting billions of people[12–14].

Understanding how the Earth's climate system naturally regulates atmospheric CO_2 concentrations is critical to addressing this crisis. Documented orbital cyclicity imprinted in pCO_2, temperature and ice volume archives over the last 800,000 years[2,15–18] suggests that these variations respond to Earth's orbital cycles[19]. These orbital variations affect the distribution and intensity of received solar radiation, producing significant changes in global climate. It has been widely accepted that summer insolation at 65°N, largely controlled by precession, is crucial for glacial-interglacial cyclicity because it significantly influences whether snow and ice are preserved over the summer. The preservation (or melting) of ice in the Northern Hemisphere, in turn, affects global climate patterns[19–22], which is the basis of the Milankovitch theory[16,19,20].

However, the full extent of these climate shifts cannot be explained by orbital cycles alone. They are further amplified or moderated by feedback mechanisms, including oceanic physical and biogeochemical processes[23,24]. One of the key feedback mechanisms is the biological pump, which is an important piece in the puzzle modulating atmospheric pCO_2 levels[23,25]. The biological pump involves the production of organic matter by phytoplankton in the surface ocean, which after dying, sinks to the deep ocean. This process removes inorganic carbon from the upper layer and transfers it to the seafloor, which in turn allows the upper layer to absorb more CO_2 from the atmosphere, decreasing its concentration on it, while storing it in the sediments and bottom waters[26]. This process interacts with other feedback mechanisms, such as changes in Antarctic ice sheets, gas outgassing, southwesterly winds and iron fertilisation[27,28]. Altogether, these processes modulate atmospheric pCO_2 concentrations during the glacial-interglacial periods of the Quaternary.

Marine calcifying plankton (e.g., coccolithophores and planktonic foraminifera) contributes to part of the organic matter and carbonate reaching the seafloor in the open oceans[29]. Planktonic foraminifera in particular are excellent archives of past ocean and climate conditions because their calcite tests record changes in temperature, salinity, and carbonate chemistry over time. However, the calcite fluxes from these organisms suffer considerable dissolution as they descend through the water column and settle on the sediments. This dissolution is driven by factors such as metabolic CO_2 release in shallow waters and the solubility of calcite in deeper waters[30]. In the Atlantic Ocean, the preservation or dissolution of carbonate at the seafloor is influenced by the saturation state of bottom water masses with respect to carbonate ions, which varies depending on their origin. Northern Component Water (NCW) tends to be saturated in carbonate ions, thereby promoting carbonate preservation. In contrast, Southern Component Water (SCW) is often undersaturated in carbonate ions, leading to increased carbonate dissolution at the seafloor[31]. The spatial extend and efficiency of these dissolution patterns have likely varied through Earth's history, influenced by changes in primary productivity and bottom water mass geometry. For instance, biologically mediated dissolution has been recorded in the eastern South Atlantic[32] and Indian Ocean[33], particularly during large upwelling events associated with precession changes. The decomposition of organic matter by bacteria and other microorganisms produces CO_2, further enhancing carbonate dissolution by lowering the pH of the surrounding water[34,35]. A schematic illustration of the processes influencing carbonate dissolution in marine environments is shown in **Figure 1**.

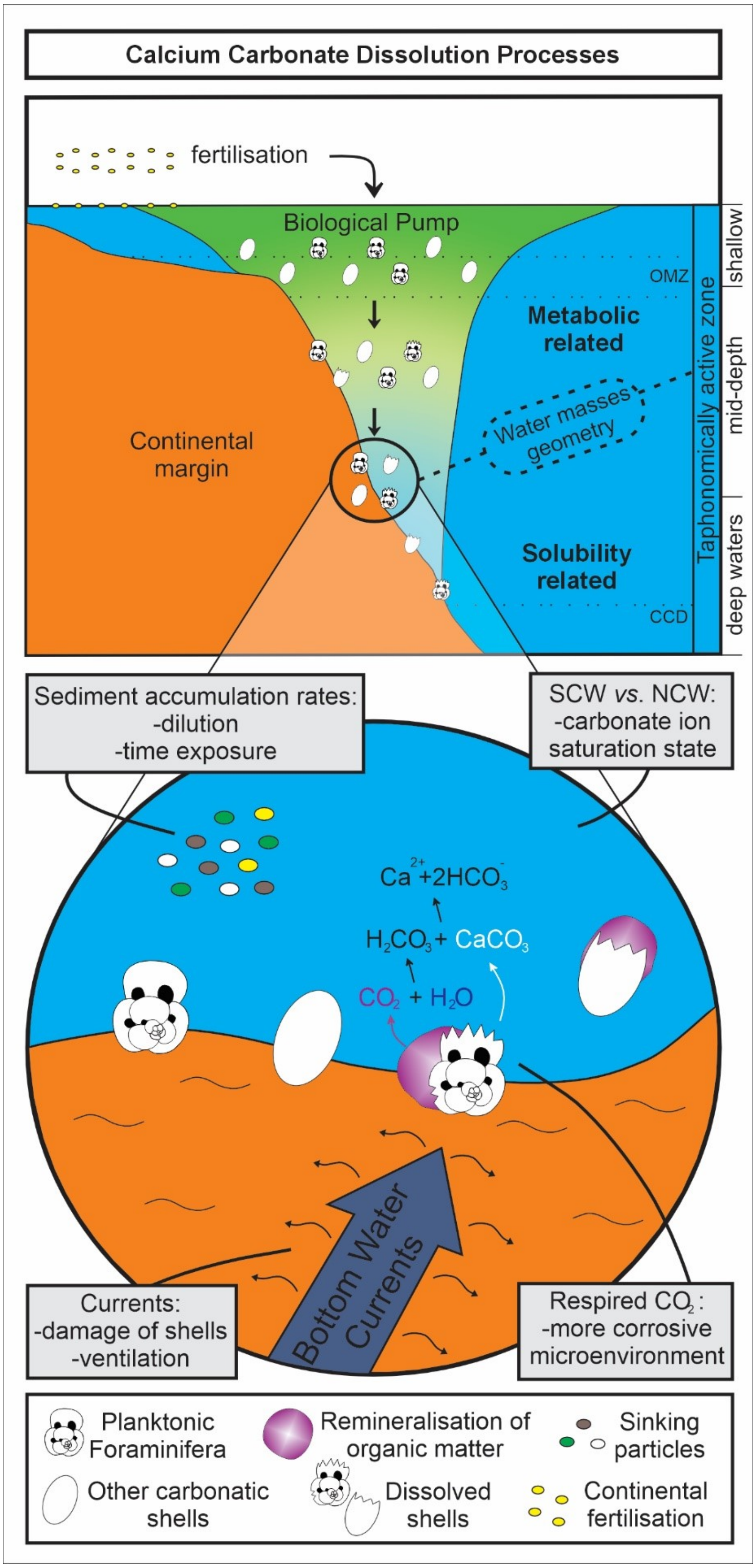

Figure 1. Scheme representing key factors contributing to the dynamics of calcium carbonate ($CaCO_3$) dissolution and preservation[30] across a depth transect through the

Brazilian continental margin. Top panel: terrestrial fertilisation enhances the biological pump by increasing nutrient supply, which enhances primary productivity and supports the growth of planktonic foraminifera and other marine organisms. Organic matter produced in the surface ocean sinks, contributing to biologically mediated carbonate dissolution as it descends and remineralises through the water column. Variations in water masses and the oxygen minimum zone (OMZ) also influence carbonate dissolution. As planktonic foraminifera tests suffer post-mortem effects already in the water column, it already constitutes the taphonomically active zone[35]. Middle panel: Processes such as sediment accumulation (which affects carbonate content by dilution and exposure time) and water mass geometry (SCW *vs*. NCW, Southern *vs*. Northern Component Water) play roles in carbonate preservation[31]. Bottom panel: Organic matter remineralisation produces CO_2, creating a corrosive microenvironment that promotes further shell dissolution, while at the seafloor, bottom water currents can transport and damage carbonate shells and affect ventilation. These processes, altogether, determine carbonate preservation or dissolution in marine sediments.

More recently, increasing numbers of studies suggest that obliquity plays a key role in modulating the extent and variability of southern hemisphere ice sheets[25,36–38]. Low obliquity values have been linked to lower temperatures due to less solar radiation received during summer[25,39], reducing ice melting and allowing ice sheets to build up over time[40]. This expansion of ice sheets also enhances the delivery of ice-rafted debris[41] (IRD). The expansion of sea ice sheets can create a positive feedback loop by increasing the albedo effect, further cooling down the surface, and promoting more ice formation[2,20]. This process also affects the ocean-atmosphere exchange, reducing the CO_2 degassing of circumpolar deep waters into the atmosphere, trapping and dissolving more CO_2, while producing more corrosive SCW[42–44]. The equatorward expansion of Antarctic Sea ice sheets has been interpreted from IRD index (core TN057-6[45]) and sodium concentration from Vostok core[46], which can give a time-spatial notion of ice sheet extensions and latitudinal position of the northern limit of southwesterly winds. Key sites for these models are East Antarctica (EPICA Dome C and Vostok ice cores) and the southeast Atlantic (ODP 1090), with tight correlations in temperature changes and dust fluxes. Iron fertilisation in the subantarctic zone would have boosted phytoplankton production, in response to a northern position of the southwesterly wind belt, which in turn enhanced nitrate consumption, recorded in $\delta^{15}N$ of foraminiferal bounds[28]. Although Patagonian dust fertilisation has been well documented on the southeast Atlantic[47], studies from the southwest Atlantic are sparse, with studies concentred in subtropical latitudes.

Given this dynamics, the past 130,000 years (Marine Isotope Stages, MIS, 5 – 1) have witnessed extreme and well documented climatic changes[2,18,48], providing an excellent opportunity to investigate the interplay between feedback mechanisms and Earth's climate system, particularly during glacial and interglacial periods. In the western south Atlantic, particularly along the southeastern Brazilian continental margin, increased productivity during the last interglacial period, Marine Isotope Stage (MIS) 5, has been well documented[49–52]. This increase in productivity has been identified through studies that utilised relative abundances of *Globigerina bulloides*, a eutrophic planktonic foraminifera species that serves as an indicator of surface productivity[53,54], suggesting intense upwelling events at the onset of MIS 5[49–51]. These events occurred within a large, expanding and retreating western boundary upwelling system, spanning 20 to 28°S, and were driven by variations in seasonal amplitude modulated by the eccentricity cycle[51,52]. Additionally, similar offshore-expanded upwelling events have been observed during other interglacial stages with high eccentricity, underscoring the role of orbital eccentricity as a dominant factor[52]. These findings suggest that such upwelling expansions likely had a significant impact on marine productivity, organic matter export and carbon accumulation, although the extent to which these expanded regional upwelling events can counterbalance atmospheric CO_2 levels has not been quantified yet.

Furthermore, in the southernmost Brazilian continental margin, enhanced productivity has been documented for the last glacial stage[55,56], primarily due to the upwelling of nutrient rich subsurface waters and continental fertilisation, which have been linked to Antarctic's dynamics[57]. However, there is a notable lack of studies using planktonic foraminifera to study the last interglacial stage, leaving the southern extent of the abovementioned upwelling events in this region less understood. If the fertilisation in the southern Brazilian continental margin was synchronised with the Southern Ocean's dynamics, such as the northward displacement of the southwesterly winds[58], it could have enhanced dust-borne iron fertilisation. This process, combined with winter intrusions of terrestrial fluvial outputs, would have fertilised the area, especially during periods of lower relative sea levels[56]. As a result, the enhanced biological pump in the western south

Atlantic would likely have contributed significantly to the glacial carbon sink by exporting organic matter to the seafloor. This increased carbon sequestration could have played a key role in the global marine carbon cycle and, by extension, the Earth's climate system.

Problem

Given the strong contrast in climatic variation during MIS 5 – 1, and the lack of integrative studies for the southern Brazilian continental margin, this thesis aims to comprehend the fertilisation mechanisms that modulated past primary productivity. Furthermore, it also explores calcium carbonate accumulation dynamics, and how it relates to the global marine carbon cycle.

Study area

The study area is located on the continental slope of the southernmost Brazilian margin in the western South Atlantic. The region is influenced by the complex interplay of various water masses and currents, including the Brazil Current, which flows southward carrying warm and salty tropical water, and the Malvinas Current, which transports cold and fresh subantarctic water northward. These currents converge at the Brazil/Malvinas Confluence near 38°S, creating a dynamic oceanographic environment[59–61]. Surface circulation in the shelf area is dominated by the northward flowing Brazil Coastal Current, which mixes oceanic and continental drainage waters, significantly influencing nutrient distribution. Major continental sources of nutrients include the Río de la Plata Estuary and the Patos-Mirim Lagoon System[62,63].

Subsurface water masses include the South Atlantic Central Water (SACW), Antarctic Intermediate Water (AAIW), Upper Circumpolar Deep Water (UCDW), North Atlantic Deep Water (NADW), and Antarctic Bottom Water (AABW)[61]. The NADW is known for promoting carbonate preservation due to its higher carbonate ion concentration, while the UCDW and AABW are associated with carbonate dissolution due to their undersaturation in carbonate ions[31]. This diverse hydrographic setting provides a unique opportunity to study past changes in productivity, and carbonate dissolution, which are critical for understanding the biological pump and its role in the global carbon cycle during the last interglacial-glacial interval.

Objectives

- To reconstruct past variations in surface primary productivity in the study area over the 5 – 110 ka time interval, as well as to discuss possible mechanisms related to observed changes.
- To investigate calcium carbonate accumulation/dissolution dynamics and analyse them in a local/global context.
- To analyse the impact of ecological *vs*. taphonomical conditions on the test size variation of planktonic foraminifera.

Chapter 2:
About the structure of this thesis

This PhD thesis is compounded by two published articles (open access), one submitted manuscript (available as a pre-print) and this integrative text.

✓ **Article #1**:

Calcium carbonate dissolution triggered by high productivity during the last glacial-interglacial interval in the deep western South Atlantic. 2022. **Suárez-Ibarra, J.Y.**, Frozza, C.F., Palhano, P.L., Petró, S.M., Weinkauf, M.F.G., Pivel, M.A.G. *Frontiers in Earth Science*, 10:830984[64]. https://doi.org/10.3389/feart.2022.830984

My contribution: I participated in the design of the study (conceptualisation and methodology), investigation (data collection), formal analysis, curated the data, and handled visualisations. I wrote the first draft of the manuscript and worked on subsequent corrections.

✓ **Article #2**:

Surface fertilisation and organic matter delivery enhanced carbonate dissolution in the western South Atlantic. 2023. **Suárez-Ibarra, J.Y.**, Freire, T.M., Frozza, C.F., Pinho, T.M., Petró, S.M., Dias, B., Chalk, T., Chaabane, S., Srivastava, M., Costa, K., Toledo, F., de Garidel-Thoron, T., Coimbra, J.C., Pivel, M.A.G. *Frontiers in Ecology and Evolution*, 11:1238334[65]. https://doi.org/10.3389/fevo.2023.1238334

My contribution: I participated in the design of the study (conceptualisation and methodology), formal analysis, curated the data, and handled visualisations. I co-wrote the first draft of the manuscript and worked on subsequent corrections.

✓ **Submitted manuscript #1**:

Planktonic foraminifera test size dictated by conditions in life and post-mortem. **Suárez-Ibarra, J.Y.**, Vieira, I., Frozza, C.F., Chaabane, S., Palhano, P.L., Kovář, V., Chalk, T., Anjos-Zerfass, G.S., de Garidel-Thoron, T., Holcová, K., Pivel, M.A.G. *Submitted to Journal of Foraminiferal Research*[66]. https://doi.org/10.22541/au.171987328.88940417/v1.

My contribution: I participated in the design of the study (conceptualisation and methodology), formal analysis, curated the data, and handled visualisations. I co-wrote the first draft of the manuscript and worked on subsequent corrections.

Finally, although they are not part this PhD thesis, I mention other papers that I was also involved during my PhD studies. **Article I** and **Article II** originated from my master's research, specifically focused on core SAT-048A. During the first year of my PhD, I had to do additional work to get these papers published. **Article I** compares biostratigraphical schemes for the Late Quaternary in the western South Atlantic, while **Article II** aims to improve the quantification of planktonic foraminifera fragmentation. Both papers provided a foundation for the first article in this PhD thesis. I also collaborated with Brazilian colleagues on the palaeoecological interpretation of bioerosion drill holes in planktonic foraminiferal tests from the western South Atlantic, ending up in the submission of a manuscript (**Submitted Manuscript I**). Finally, as part of a collaboration with Brazilian and German researchers, we produced a manuscript on the palaeoecology of Quaternary south American megamammals (**Submitted Manuscript II**). I contributed by extracting collagen from bones at the Max Planck Institute of Geoanthropology that served to conduct isotopic analyses (carbon and oxygen), as well as participating in the manuscript review and editing.

✓ **Article I**:

Time-spatial boundaries of bioecozonations (planktonic foraminifera) in the latest Quaternary: a case study from the western South Atlantic. 2021. **Suárez-Ibarra, J.Y.**, Petró, S.M., Frozza, C.F., Freire, T.M., Portilho-Ramos, R.C., Pivel, M.A.G. R*evue de Micropaléontologie*, 73:100554[67]. https://doi.org/10.1016/j.revmic.2021.100554

✓ **Article II**:

Fragment or broken? Improving the planktonic foraminifera fragmentation assessment. 2021. **Suárez-Ibarra, J.Y.**, Frozza, C.F., Petró, S.M., Pivel, M.A.G. *Palaios*, 36(4),165-172[68]. https://doi.org/10.2110/palo.2020.062

✓ **Submitted Manuscript I**:

Where it's worth it: frequency and spatial distribution of bioerosional drill holes in planktonic foraminifera reveal different strategies in site selectivity. Frozza, C.F., **Suárez-Ibarra, J.Y.**, Matias, R., Coimbra, J., Pivel, M.A.G. *Submitted to Paleobiology on 04.01.2024.*

✓ **Submitted Manuscript II**:

França, L.D.M., de Melo, M., **Suárez-Ibarra, J.Y.**, Ziegler, M., Roberts, P., de Araújo-Junior, H., Dantas, M.A.T. Revealing two Quaternary tank deposits in the Brazilian Intertropical Region: Satellite images, fossil content, taphonomic, paleopathological, and paleoecological analyses. *Submitted to Journal of South American Earth Sciences Sciences on 29.11.2023.* https://dx.doi.org/10.2139/ssrn.4655559

Chapter 3:
Material and methods

The articles and manuscripts of this PhD thesis are based on the following piston cores:

- SAT-048A (29°11′ S; 47°15′ W; 3.54 m length; 1,542 m water depth),
- SIS-203 (29°30′S; 47°7′W; 3.60 m length; 1,894 m water depth) and,
- SIS-249 (30°05′ S; 47°05′ W; 1.94 m length; 2,091 m water depth).

The three cores were collected by *Fugro Brasil Ltda* for the *Brazilian National Agency of Petroleum* in 2007, covering different depths and time intervals of the continental slope of the southern Brazilian margin, western South Atlantic. Although their temporal coverage does not fully overlap, they allow the spatial assessment of surface and seafloor palaeoceanographic changes in the study area.

The age model of each core is based on published benthic oxygen stable isotopes ($\delta^{18}O$) and ^{14}C dates on monospecific planktonic foraminiferal samples[69–71]. These details are presented in the respective publications or supplementary materials. To compute the age model of each core, I used the package *Bacon*[72] in *R*[73] and *Rstudio*[74]. ^{14}C dates were corrected within the package using the IntCal Marine20 calibration curve[75]. The delta marine radiocarbon reservoir (ΔR = -85 ±40) was calculated with the online tool found at www.calib.org, based on regional calibrations[76–78].

Planktonic foraminiferal census counts to species level[79–81] were used to assess changes in past sea (sub)surface conditions. Past sea subsurface temperatures were reconstructed utilising the Modern Analog Technique[82] from the free software Past[83]. The calibration used 1,538 core top samples from the Atlantic Ocean (including 421 samples from the South Atlantic), recovered from the ForCenS database[84] and the Brazil-Malvinas Confluence area[85]. Temperatures were extracted from the World Ocean Atlas 2013[86], using the Ocean Data View software[87]. Primary productivity was assessed using the relative abundances of *Globigerina bulloides*, *Globigerinita glutinata* and the *G. bulloides* to *Globigerinoides ruber* (*G. ruber albus*, *G. ruber ruber* and *G. elongatus* complex) ratio[88,89]. Planktonic $\delta^{18}O$ isotopes were used to reconstruct upper water column stratification and sea surface salinity through the oxygen residual method.

Benthic to planktonic foraminifera ratio was used to infer changes in past organic matter export to the sea-floor conditions (mid-depth core SAT-048A) and carbonate dissolution (deeper cores SIS-203 and SIS-249). The number of whole planktonic foraminifera tests per gram of dry sediment, the degree of planktonic foraminifera fragmentation, the calcium carbonate content and the coarse sediment fraction (>0.63 µm) were analysed to quantify the carbonate dissolution.

Neodymium isotope ratios (εNd) from planktonic foraminifera oxide coatings were measured in this study to reconstruct water mass influences. This because εNd serves as an effective quasi-conservative[90] tracer for studying water masses, as the isotopic signatures are influenced by the geological origins of the regions from which the water flows. When foraminiferal tests settle on the seafloor, oxides precipitate on their surfaces, embedding the Nd from the bottom waters. This process allows the oxide coatings to reflect the εNd signature of the water mass. Different water masses have characteristic εNd signatures. For instance, northern component water (North Atlantic Deep Water) typically shows less radiogenic εNd values ranging from -13 to -10, while southern component water (Antarctic Bottom Water) displays more radiogenic values between -8 and -6[91–94].

Chapter 4:
Main results

This section provides an overview of the changes observed in palaeoproductivity and carbonate dissolution in the southernmost Brazilian continental margin, western South Atlantic, during MIS 5 to MIS 1, with a focus on their potential interrelations. The discussion is organised by similarities in the process (primary productivity, carbonate metabolic- and solubility-related dissolution), distinguishing between glacial and interglacial periods, and incorporates comparisons with other records, particularly those from the western South Atlantic and Southern Hemisphere.

Palaeoproductivity changes in the western South Atlantic during MIS 5 – 1

This project's findings indicate that the southernmost Brazilian continental margin experienced higher glacial (MIS 2 – 4) sea surface productivity, as recorded by cores SAT-048A, SIS-203 and SIS-249[64,65]. These results are in agreement with previous studies [55,95–98], which also reported elevated productivity during the last glacial period in this region. A preliminary model by Mahiques et al.[98] is proposed to explain these past productivity changes, considering the relative position of the Brazil Current. This model states that low relative sea levels and an offshore shift of the Brazil Current would influence terrigenous nutrients input (for a core retrieved at ~24°S)[98]. Mahiques' et al.[98] concept has been updated and refined through time to be applied in other areas, including the important of the Brazil Current, where its intensity and meandering influences (coastal, Ekman and/or shelf-break) upwelling processes, pumping to (sub)surface nutrient-rich south Atlantic central water that fertilises the photic layers[99–103].

In contrast, the southeast region, between latitudes 20 and 23°S, exhibited different productivity patterns[49,50]. Going back in time to last, high productivity due to elevated upwelling was also documented in the southeastern Brazilian continental margin (cores GL-74 and GL-75), invoking again the influence of a low relative sea level, coupled with strengthened NE winds[49]. This high productivity during the last interglacial was also documented using coccolithophore records[104]. However, another study covering MIS 5 and 6[105] (core GL-1090), provided evidence that the relative sea level did not influence past expanded upwelling events but the intensity of the Brazil Current, related to eccentricity maximum and stronger NE winds. Later, another study located relatively southern (core JPC-17)[56], argued that the proposed orbital mechanism could not trigger the glacial upwelling expansions of the southern Brazilian continental margin. Instead, the authors propose an interplay between SW winds, carrying from the south La Plata plume water during winters, and NE winds, pumping south Atlantic central water rich in silicic acid ($Si(OH)_4$) during summers. Data from the southern cores SAT-048A[64] and SIS-188[106] partially agrees with the abovementioned hypothesis, as several palaeoproductivity indicators seem to vary following the summer insolation.

Another study analysing cores GL-852 and GL-854 found significant 100-kyr cycles in the expansion of past upwelling events on the southeastern Brazilian margin[52], corroborating the hypothesis of expanded upwelling under high eccentricity values until MIS 18 (770 ka). However, this patter was not observed during MIS 1 and 11, when eccentricity values are too low to generate a strong seasonal difference in the winds. Previously, it was established that relative abundances of *G. bulloides* (>10%) or *Gb*/*Gr* (>0.2) could be related to increased upwelling events[52,53,105,107–110]. Therefore, quantifying the presence of *G. bulloides* can be helpful to constrain, in time and space, past upwelling events. Putting together, published records of *Globigerina bulloides* abundances and *G. bulloides* and *Globigerinoides ruber* (*Gb*/*Gr*) ratio from the southern and southeast Brazilian margin (between 20 and 30°S, **Table 1**, **Figure 2**), it is possible to see, with suborbital scale variation, high productivity during i) the last interglacial and ii) the last glacial. Although sediment records from the southernmost part are not old enough to document changes in the abundance of *G. bulloides* during the MIS 6 – 5 boundary, it is possible to see two main latitudinal differences. The first is that upwelling events were stronger and delayed in the southeast part, and rather weak and constant through the MIS 5 – 4 boundary for the southern portion (**figures 3 and 4**). The second is during the glacial, which seems weak and confined to the MIS 3 – 2 boundary in the southeast, and stronger and widespread throughout the glacial (MIS 2 – 4) in the south (**figures 3 and 4**). However, given the "fragmentary" nature of the sedimentary records from the southernmost part, it urges to find and study complete and longer temporal cores. These observations emphasise distinct latitudinal influences on surface primary productivity and suggest a need for further investigation into the temporal and spatial dynamics of productivity in the southernmost part of the study area.

Table 1. This table provides the geographic coordinates (longitude and latitude) and respective depths in meters below sea level (mbsl) of nearby sediment cores (**Figure 2**).

Core	Longitude	Latitude	Depth (mbsl)
M125-55-7[111]	-38.62	-20.36	1,960
GL-75[49]	-40.02	-21.14	1,421
GL-77[50]	-40.04	-21.2	1,287
GL-74[49]	-40.04	-21.25	1,279
KF-I[112]	-42.3	-24.44	1,682
KF-H[113]	-42.54	-24.53	1,695
NAP63-1[96]	-44.31	-24.83	842
GL-1090[51]	-42.51	-24.92	2,225
GL-852[52]	-43.55	-25.01	1,938
GL-854[52]	-42.61	-25.2	2,220
GeoB2107-3[55]	-46.45	-27.17	1,048
JPC-17[56]	-46.49	-27.69	1,627
SAT-048A[64]	-47.25	-29.19	1,542
SIS-188[114]	-47.47	-29.37	1,514
SIS-203	-47.1	-29.5	1,894
SIS-249[65]	-47.08	-30.08	2,091

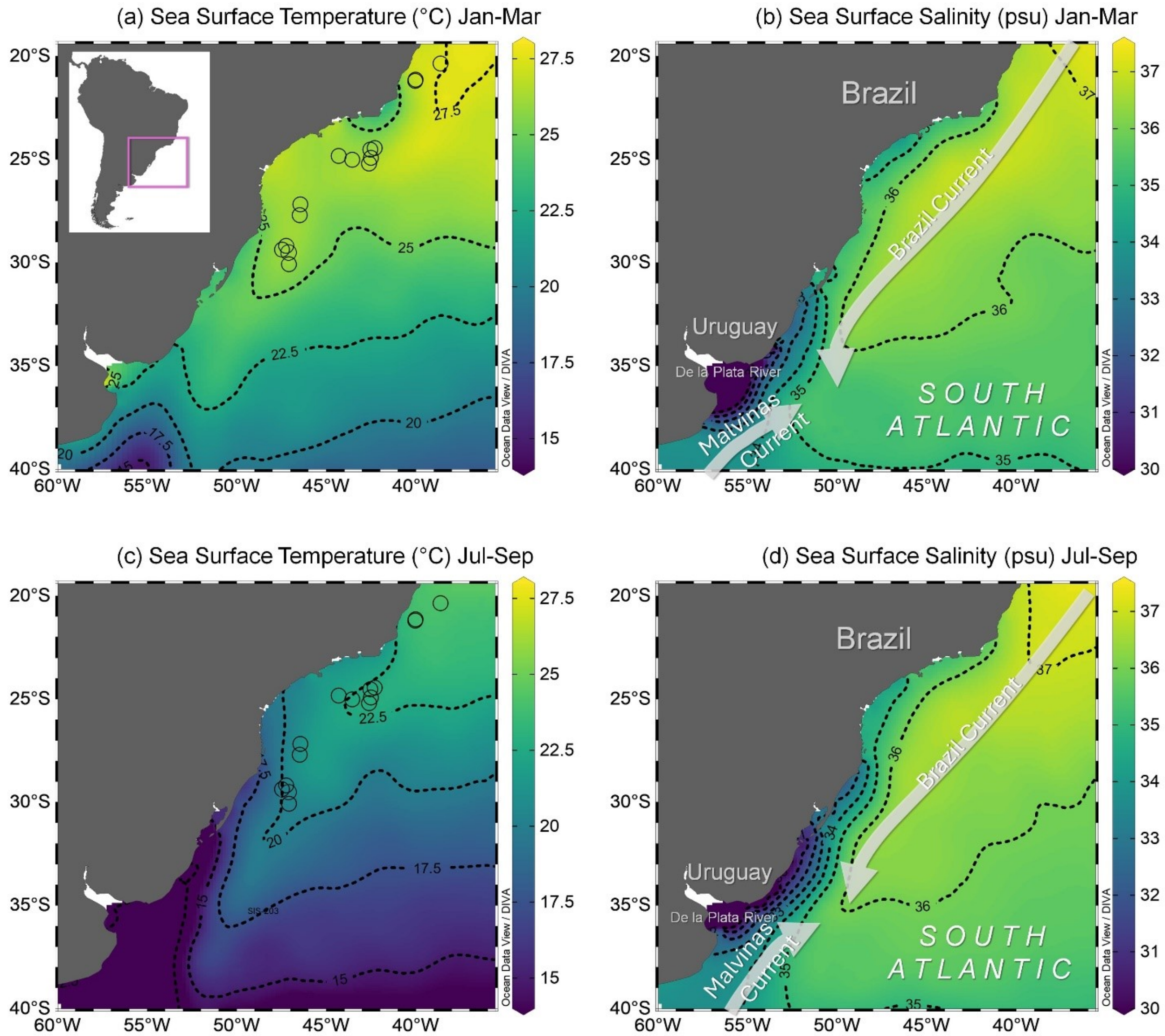

Figure 2. Geographical distribution of nearby sediment cores along the southeast (~23°S) and southern (~30°S) Brazilian continental margin (**Table 1**). Top panel shows sea surface temperature[86] (a) and salinity[115] (b) for austral summer (from January to March), while bottom panel shows temperature (c) and salinity (d) for austral winter (from July to September). The Brazil Current flows southward along the coastline transporting warm water at the Malvinas Current flows northward transporting cool water. Outflows from De la Plata River affects salinity in the study area on a seasonal basis. Figure made with Ocean Data View[87].

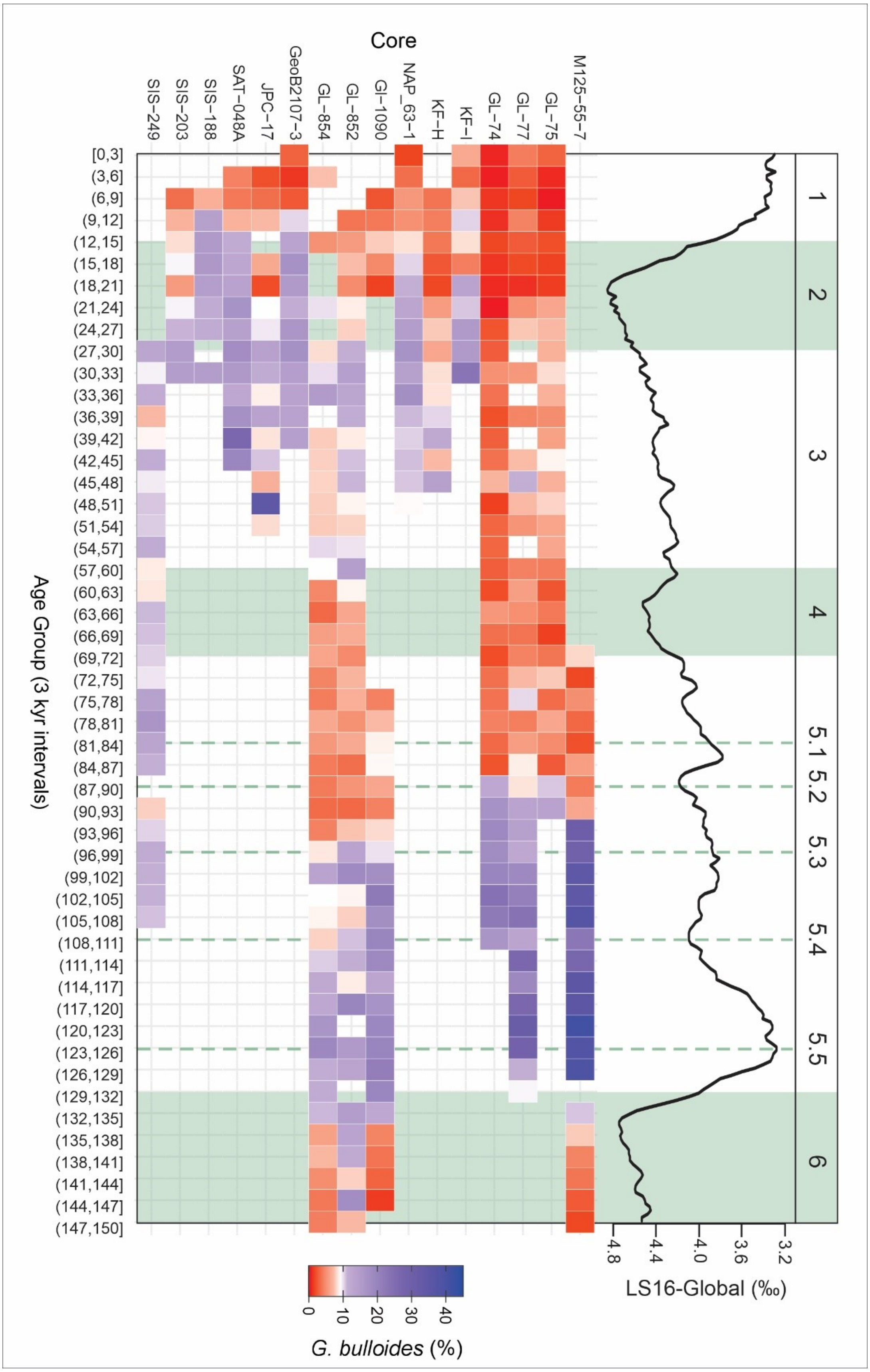
Core
SIS−249
SIS−203
SIS−188
SAT−048A
JPC−17
GeoB2107−3
GL−854
GL−852
GI−1090
NAP_63−1
KF−H
KF−I
GL−74
GL−77
GL−75
M125−55−7
Age Group (3 kyr intervals)
[0,3]
(3,6]
(6,9]
(9,12]
(12,15]
(15,18]
(18,21]
(21,24]
(24,27]
(27,30]
(30,33]
(33,36]
(36,39]
(39,42]
(42,45]
(45,48]
(48,51]
(51,54]
(54,57]
(57,60]
(60,63]
(63,66]
(66,69]
(69,72]
(72,75]
(75,78]
(78,81]
(81,84]
(84,87]
(87,90]
(90,93]
(93,96]
(96,99]
(99,102]
(102,105]
(105,108]
(108,111]
(111,114]
(114,117]
(117,120]
(120,123]
(123,126]
(126,129]
(129,132]
(132,135]
(135,138]
(138,141]
(141,144]
(144,147]
(147,150]
1
2
3
4
5.1
5.2
5.3
5.4
5.5
6
4.8
4.4
4.0
3.6
3.2
LS16-Global (‰)
0
10
20
30
40
G. bulloides (%)

Figure 3. Heatmap of *Globigerina bulloides* relative abundances in sediment cores from the south/east Brazilian Margin and the $\delta^{18}O$ LS16-Global[116]. Cores are organised through a latitudinal transect from north to south: M125-55-7[111], GL-74, GL-75[49], GL-77[50], KF-I[112], KF-H[113], NAP-63-1[96], GL-1090[51], GL-852, GL-854[52], GeoB2107-3[55], JPC-17[56], SAT-048A[64], SIS-188[117], SIS-203 and SIS-249[65]. Over time, the scale colour shows the relative abundance of *G. bulloides* in various sediment cores (*y*-axis) across different age intervals (*x*-axis, binned by 3 kyr). Warmer colours (red) indicate lower abundance, associated with lower nutrient availability, while cooler colours (blue) represent higher abundance and higher nutrient availability. A sharp transition occurs at 10%, as this value serves as a critical threshold indicating significant shifts in nutrient supply and upwelling intensity[52,53,105,107–110].

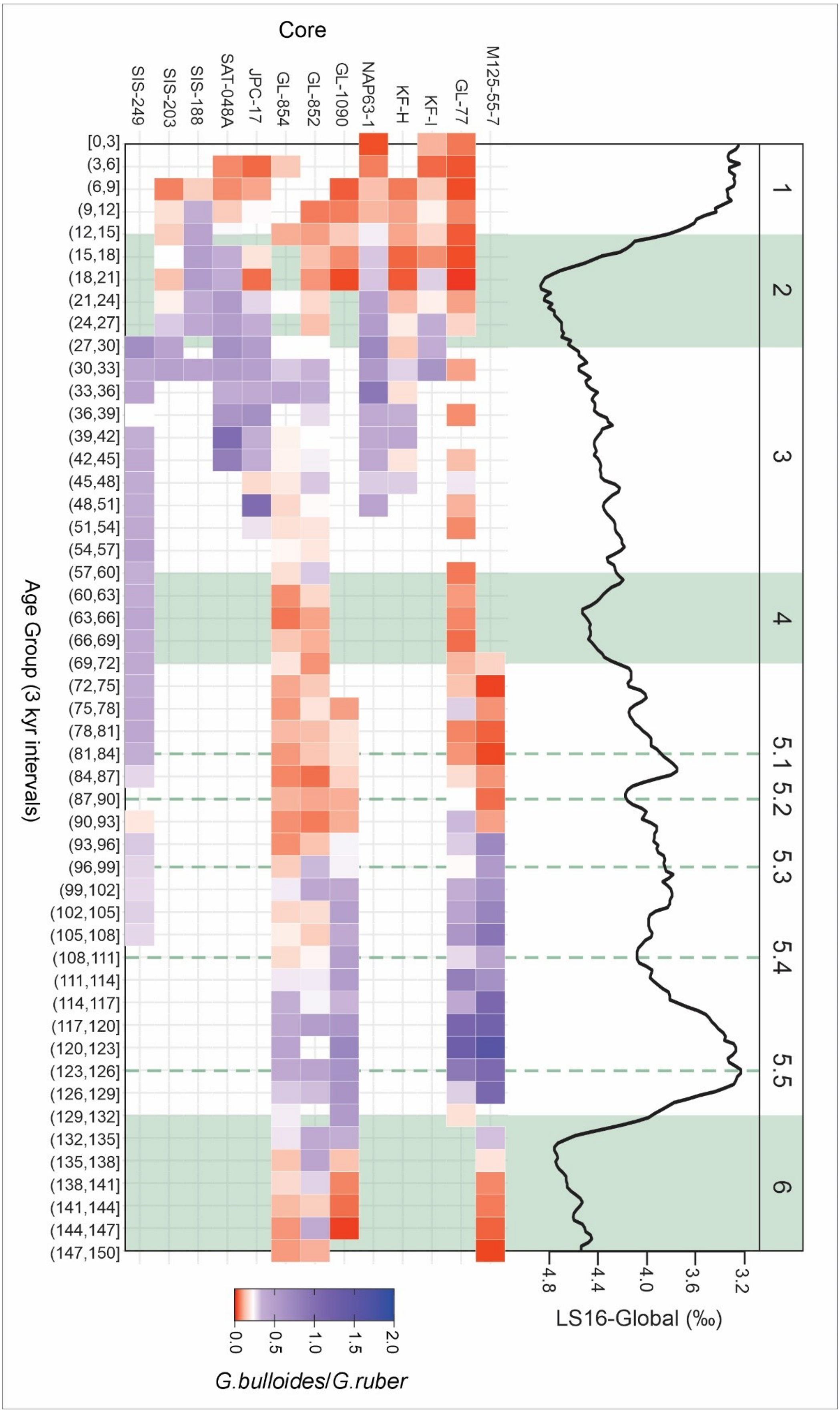
Core
SIS-249
SIS-203
SIS-188
SAT-048A
JPC-17
GL-854
GL-852
GL-1090
NAP63-1
KF-H
KF-I
GL-77
M125-55-7
Age Group (3 kyr intervals)
[0,3]
(3,6]
(6,9]
(9,12]
(12,15]
(15,18]
(18,21]
(21,24]
(24,27]
(27,30]
(30,33]
(33,36]
(36,39]
(39,42]
(42,45]
(45,48]
(48,51]
(51,54]
(54,57]
(57,60]
(60,63]
(63,66]
(66,69]
(69,72]
(72,75]
(75,78]
(78,81]
(81,84]
(84,87]
(87,90]
(90,93]
(93,96]
(96,99]
(99,102]
(102,105]
(105,108]
(108,111]
(111,114]
(114,117]
(117,120]
(120,123]
(123,126]
(126,129]
(129,132]
(132,135]
(135,138]
(138,141]
(141,144]
(144,147]
(147,150]
1
2
3
4
5.1
5.2
5.3
5.4
5.5
6
4.8
4.4
4.0
3.6
3.2
LS16-Global (‰)
0.0
0.5
1.0
1.5
2.0
G.bulloides/G.ruber

Figure 4 Heatmap of *Globigerina bulloides* and *Globigerinoides ruber* ratio in sediment cores from the south/east Brazilian Margin and the $\delta^{18}O$ LS16-Global[116]. Cores are organised through a latitudinal transect from north to south: M125-55-7[111], GL-74, GL-75[49], GL-77[50], KF-I[112], KF-H[113], NAP-63-1[96], GL-1090[51], GL-852, GL-854[52], GeoB2107-3[55], JPC-17[56], SAT-048A[64], SIS-188[117], SIS-203 and SIS-249[65]. Over time, the scale colour shows the ratio between *G. bulloides* and *G. ruber* in various sediment cores (*y*-axis) across different age intervals (*x*-axis, binned by 3 kyr). Warmer colours (red) indicate lower abundance, associated with lower nutrient availability, while cooler colours (blue) represent higher abundance and higher nutrient availability. A sharp transition occurs at 0.2%, as this value serves as a critical threshold indicating significant shifts in nutrient supply and upwelling intensity[52,53,105,107–110].

As core SIS-249 from the southern region does not cover the entirety of MIS 5[65], I will focus on the differences observed during the last glacial period. Once again, increases in *G. bulloides* and *G.bulloides*/*G.ruber* from the compiled cores, although fragmented, seem to indicate the influence of a stronger fertilisation on the south and weaker to the southeast (**figures 3 and 4**). This difference might be due to the varying influence of low *vs*. mid to high latitudes, as previously documented for the southeast region (~23 and 24°S)[118]. This explanation is supported by the spatial variability observed between the platform and slope in cores RJ-1501 and RJ-1502, which are at depths of 328 and 1,598 mbsl respectively, and show contrasting surface conditions for MIS 2. The authors interpreted cooler and fresher water conditions related to the La Plata plume in the shallower core during the Last Glacial Maximum and the Last deglaciation, in opposition to offshore warmer and saltier water conditions of the Brazil Current[118].

While lower relative sea levels and winter intrusions of La Plata plume fertilise the photic zone of the study area during the glacial[56,118–120], it is not the sole mechanism related to strengthening south westerly winds. A mineralogical study on core SIS-249[57] suggested that dust-borne wind-driven fertilisation could explain both high glacial productivity and changes in grain size and mineralogy through MIS 5 – 2. Considering all this, the enhanced fertilisation in the southeast Brazilian margin during the last interglacial epoch might respond to a higher influence of low latitude processes responding to the eccentricity cycle, with a restricted effect on the southernmost Brazilian margin[52,105]. On the other hand, the southernmost part seems to be affected by mid-high latitudes processes, likely responding to the obliquity cycle, not powerful enough to reach till 20°S. Finally, all records indicate that primary productivity was low during the MIS 1 (**figures 3 and 4**), either by low eccentricity values[51,52], a reduced continental fertilisation[56], or a less offshore position of the Brazil current[98,121]. As the exact interaction between these processes remains unclear, further research is necessary to better understand the dynamics and interplay between these different latitudinal influences.

Calcium carbonate dynamics I: metabolic related dissolution

Proxies from sediment core SAT-048A, recovered at 1,542 m from the southern Brazilian margin, suggest that surface primary productivity responded to changes in summer insolation and NE winds[64]. Similarly, two long records from the eastern equatorial Atlantic[122] and Indian ocean[33] documented increased carbonate dissolution during periods of high surface productivity, both following changes in the precession cycles. Although the validity of this mechanism in the western South Atlantic should be tested with longer temporal records, if widespread, the expansion of the biological pump may suggest a dynamic of carbon transfer between the atmosphere and oceans reservoirs clearly modulated by the precession cycle.

Building on this, the remineralisation and subsequent dissolution processes are important to measure the effectiveness of the biological pump, as they remove carbon (organic matter and carbonate) that could potentially be buried in the sediments, recycling it and putting it back to the system[64]. Nevertheless, high productivity periods have been associated with higher accumulation rates, as well as with high total organic carbon fluxes[65,98,121]. Although biologically mediated dissolution was inferred for core SIS-249, lower temporal resolution of dissolution proxies makes its relationship with surface productivity ambiguous (**Figure 5**), as there might be a lag of 11 kyr between changes in surface productivity and carbonate dissolution (both cores SIS-203 and SIS-249), suggesting a different mechanism driving carbonate dissolution at larger depths (~2,000).

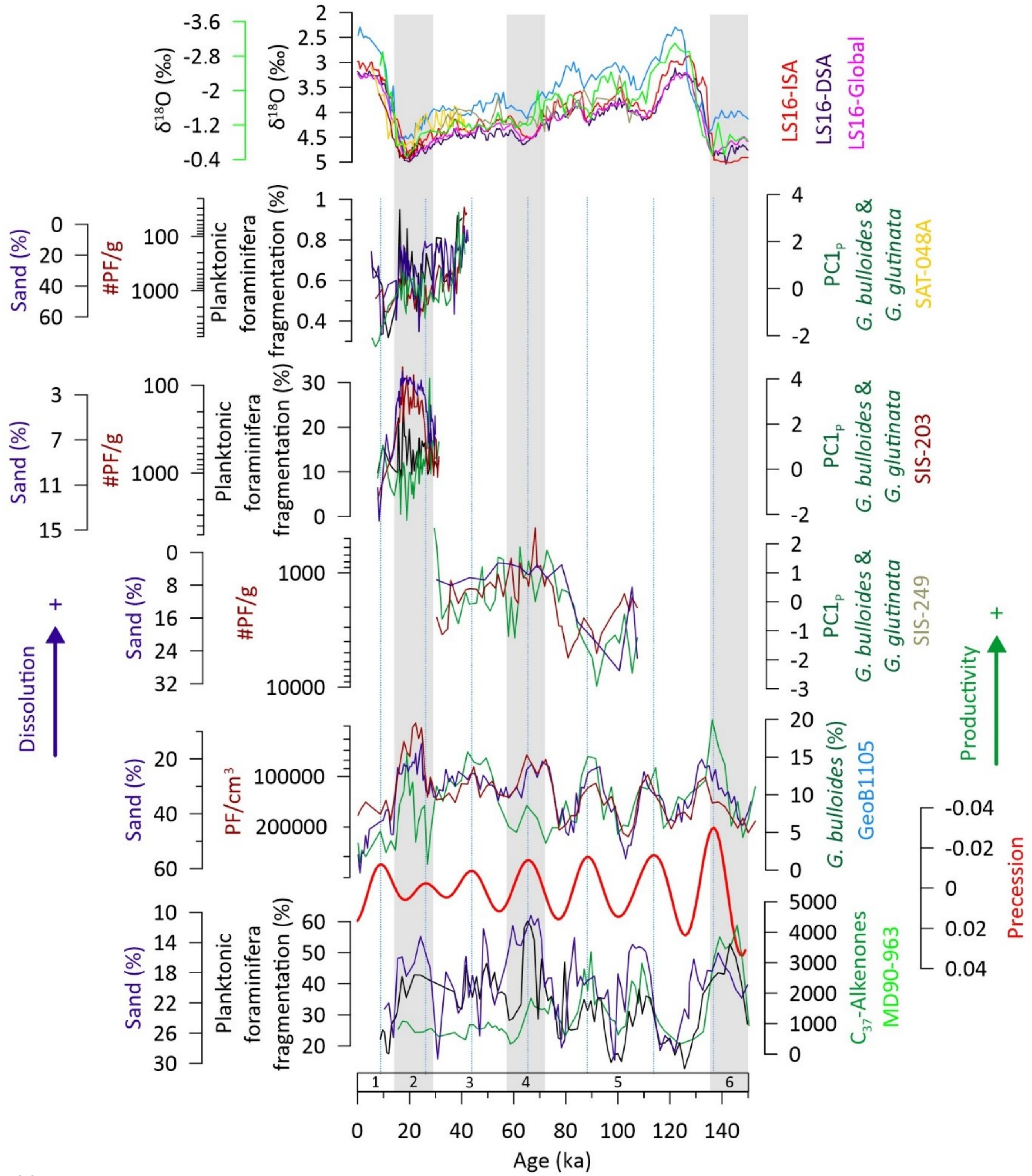

Figure 5. This figure displays the variations in oxygen isotope ratios ($\delta^{18}O$), planktonic foraminiferal fragmentation, sand content, and foraminiferal concentrations across different sediment cores during the late Quaternary. The $\delta^{18}O$ records are shown for LS-16 (ISA, DSA and Global)[116] and sediment cores identified by colour, with all cores related to the black axis except for core MD90-963, which corresponds to the green axis.

Precession values were computed from Laskar et al.[123] Highlighted grey bars represent Marine Isotope Stages (MIS) 2, 4, and 6. Data from cores SAT-048A, SIS-203, SIS-249, GeoB1105[122] and MD90-963[33] illustrate the relationship between ocean productivity, carbonate dissolution, and climatic variations over the past 150 kyr.

Calcium carbonate dynamics II: solubility related dissolution

Although cores SIS-203 (~1,894 mbsl) and SIS-249 (~2,091 mbsl) are not at exactly the same depth, they are located in close proximity to each other, with a depth difference of about 200 meters. For this study, I analysed them as a single record of deep-sea floor conditions at the study site (~2,000 mbsl) in a global context (**Figure 6**), focusing on the southern hemisphere[24,124]. When analysed together, carbonate dissolution proxies from cores SIS-203 and SIS-249 and other deep cores from the Atlantic Ocean have a similar variation (**Figure 6**), following a glacial-interglacial dynamics[122] and depicting what is called an "Atlantic carbonate accumulation type"[125].

This glacial-interglacial dynamic, driven by orbital cycles such as obliquity, plays a crucial role in modulating the processes that affect carbonate dissolution in the deep ocean. Low obliquity reduces summer solar radiation, leading to cooler temperatures, less ice melt, and the buildup of ice sheets[25,39]. This ice growth increases the Earth's albedo, creating a positive feedback loop that further cools the surface and promotes more ice formation[2,20]. The mentioned cooling process strengthened and displaced to the north (up to 40°) the south westerly winds, enhancing iron dust-borne fertilisation of the subantarctic zone[27,28,47,58,126–129], enhancing the biological pump and carbon export and remineralisation at the seafloor[44,130–132]. The already enhanced subantarctic biological pump might have expanded the organic carbon export to the seafloor by cooler Southern Ocean temperatures, as it has been shown that cooler temperatures affect metabolism, decreasing the remineralisation process through the water column[133], increasing even more the delivered organic matter and recharging the deep-ocean carbon pool[44].

At the same time, expanded sea ice sheets enhance the production of corrosive Antarctic bottom waters, here called southern component waters, evidenced by more radiogenic values in authigenic εNd[134] in core GeoB3808-6[135] and core SIS-203. With the higher presence of southern component waters, although originally subsaturated in carbonate ion, with the organic carbon rain and posterior remineralisation, they accumulate respired carbon[136] (i.e., benthic $\delta^{13}C$ GeoB3808-6[135]). The expansion of the carbon-charged component waters leads to dissolution of the exported calcareous marine plankton tests at deep depths. This dissolution is evident in dissolution proxies from cores SIS-203 and SIS-249 (western South Atlantic), TN057-6[45], ODP 1090 and GeoB1035[122] (eastern South Atlantic), ODP 108-663A[32] (equatorial Atlantic) and IODP U1313[137] (North Atlantic). The expansion of Antarctic bottom water to the deep North Atlantic[92], and of Pacific deep water to the deep South Atlantic evidenced by εNd in core MD07-3076[138], may acted as a carbon reservoir, isolating and sequestrating carbon from the atmosphere in the deep oceans.

Besides, the expansion of Antarctic Sea ice sheets might aid the higher production of southern component water by decreasing the circulation at surface through the Agulhas Leakage[139,140]. As less warm water passes through this Indo-Atlantic connection, the thermal (and salty) capacity of the South Atlantic to heat the North Atlantic through the Equatorial Current decreases, which in turn, decreases the formation of North Atlantic deep water, making space for the expansion of southern component waters.

As to the larger processes at play, if obliquity plays an important role as a tipping point of glacial-interglacial variability (termination II and I), why its low values at around 125 and 70 ka did not produce the same cascade of effects on the cryo-biosphere and chemical composition of the deep Atlantic? To answer this, I bring the following reasonings. First, because effects of precession and obliquity forcings cancel each other, so the ice sheets grow more than what they expand[38]. Second, as snow accumulates and ice sheet grows, it also spreads outward, enhancing ice flow dynamics and along with lower sea levels, the ice sheets continue to expand. Low obliquity values at 125 ka and high January insolation at 65°S may propitiate the growing of ice but not the equatorward expansion, respectively, as recorded by the sodium content from EPICA Dome C[126] core and IRD index core TN057-6[45]. In contrast, after a large accumulation of ice, when obliquity and January insolation at 65°S start to increase in phase, heat accumulation can "catastrophically" decrease the continental ice sheets[141,142], allowing the degassing of southern waters and releasing CO_2 from the oceans to the atmosphere. Interestingly, when normalised values (value minus dataset mean divided by dataset standard deviation) of obliquity are subtracted normalised summer insolation at 65°S, they produce a variation curve that mimics summer insolation at 65°N.

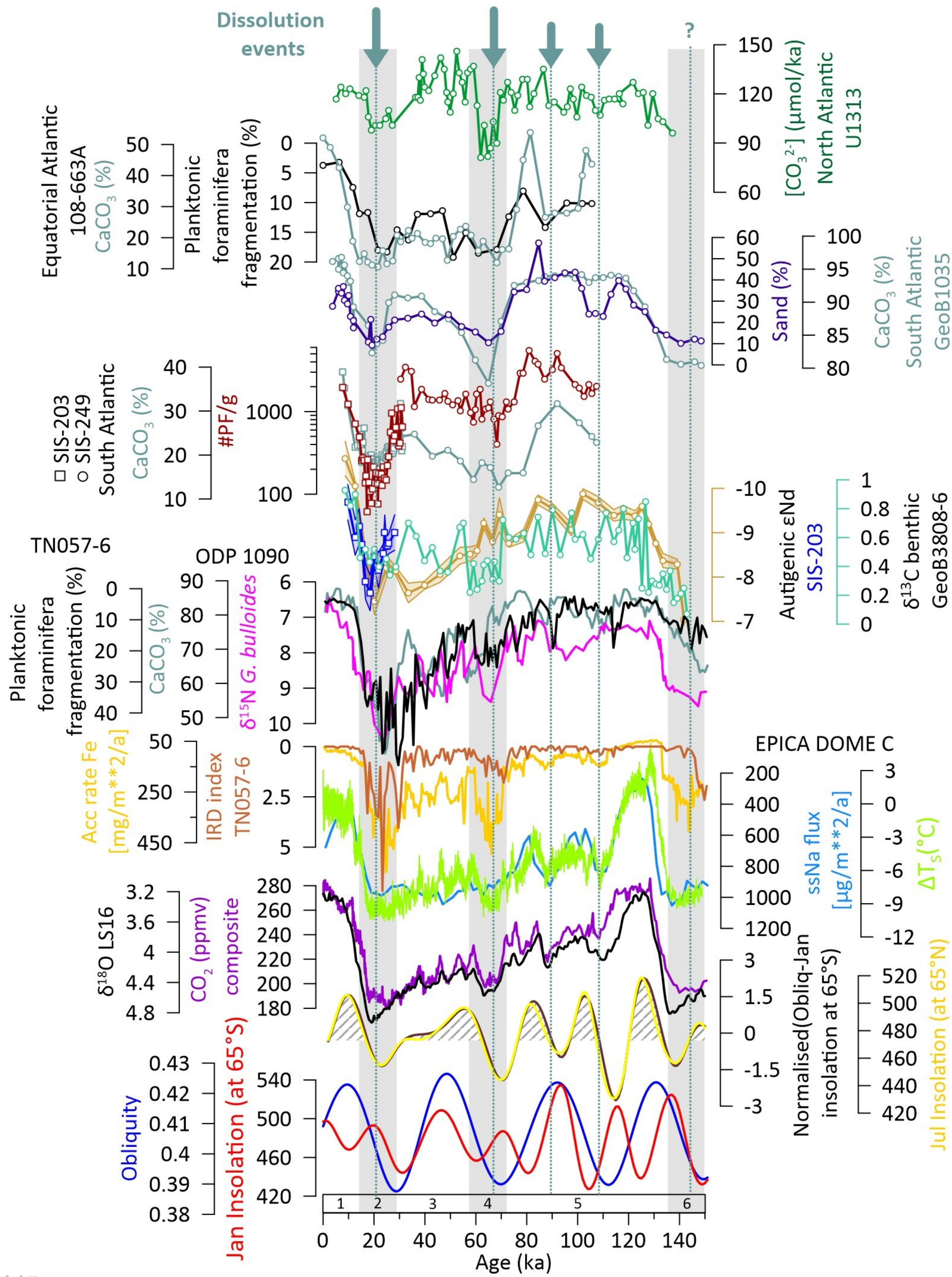

Figure 6. Multi-proxy records from various Atlantic Ocean sediment cores and Antarctic ice cores spanning the last 150,000 years. The figure shows data from the

Equatorial Atlantic (ODP 108-663A), South Atlantic (SIS-203, GeoB1035[122]), and other key locations, highlighting fluctuations in $CaCO_3$ (%), planktonic foraminifera fragmentation[45], CO_2 concentrations, IRD index[45], isotopic data ($\delta^{18}O$[116], $\delta^{13}C$[135], $\delta^{15}N$[28]), B/Ca[137], and authigenic εNd[135]. Dissolution events are marked with grey vertical bars and arrows. Obliquity and insolation curves[123] at 65°S and 65°N are included to illustrate the influence of Milankovitch cycles on glacial and interglacial periods. Temperature variations from the EPICA Dome C[143] ice core provide additional context for climate changes.

Calcium carbonate dynamics III: Its effects in planktonic foraminiferal tests

Studies point that Anthropogenic CO_2 emissions will affect marine ecosystems by shifts in biogeographical distribution and changes in species abundances[9,144–147]. Moreover, projections for calcareous plankton under elevated pCO_2 seem alarming, involving difficulties to calcify their tests[7], decreasing calcification rates[148–151], decreasing in bulk density[151,152], malformation[148], decreasing spines recovery[153], and test thinning[154] among others. Which such responses, it is expected a reduction in organic matter and calcite fluxes for marine calcareous plankton, representing a negative feedback mechanism in dissolved inorganic carbon removal, and thus impacting the global carbon cycle.

Such anthropogenic changes have already been reported to affect the calcareous plankton, when samples from current times are compared to previous or early industrial era[155–157]). Investigating the resilience and adaptability of planktonic foraminifera to past climatic changes and is vital for predicting their responses to ongoing climate change. To do so, marine sediments represent key archives with high resolution records of temperature and organisms changing rates. Nevertheless, taphonomic processes should be differentiated from ecological signals.

The study of planktonic foraminiferal test sizes from core SAT-048A[66] reveals that the relationship between size changes and environmental parameters, such as temperature and productivity, is not uniformly captured by all size descriptors. This inconsistency underscores the necessity of using multiple statistical descriptors to accurately interpret size variations, particularly in studies with low specimen counts. Using only the 95th percentile can underestimate the influence of environmental factors. Furthermore, temperature reconstructions at different depths significantly affect the relationship between temperature and test sizes, especially for species like *Globigerinoides ruber albus* and *Globigerina bulloides*. Thus, comprehensive understanding of palaeoenvironmental effects requires sensitivity tests on size descriptors and various parameters for reconstructing past environmental conditions.

Ecologically, the manuscript[66] confirms previous studies documenting that productivity is the primary driver of test size variations in planktonic foraminifera in high dynamic oceanographic areas, where nutrient availability fluctuates significantly[158]. The observed correlation between smaller *G. ruber albus* tests and increased productivity suggests reduced metabolic activity of their symbionts during upwelling periods[159]. Additionally, temperature changes in the upper water column influence test sizes, reinforcing the need for diverse temperature reconstructions.

On the other hand, the study suggests the critical role of carbonate dissolution in also reducing planktonic foraminifera test sizes by shell damage, particularly in *G. ruber albus*. High productivity periods, which increase organic matter delivery to the seafloor and respired CO_2 release, lead to lower pH levels and subsequent test dissolution. This process might be able to reduce test sizes by about 25±9%, primarily through the fragmentation and removal of thinner terminal chambers[160–162]. Such fragmentation can cause broken tests to be misidentified as smaller whole specimens, leading to underestimation of size variations. Scanning electron microscope (SEM) imaging and open-source X-ray computed micro-tomography (micro-CT) revealed that broken tests that often resemble intact ones with standard microscopy are not, making dissolution effects difficult to detect.

Chapter 5:
Glacial carbon sequestration by carbonate dynamics and biological pump in western South Atlantic

Introduction

Glacial-interglacial cycles[19,20], as observed in the orbital cyclicity of temperature changes and pCO_2 levels over in Antarctic ice cores[2,17,18,163], are intricately linked to changes in the global carbon reservoir[23,164]. However, these orbital signals alone may not fully account for the climatic changes observed, suggesting the effect of feedback mechanisms[165,166]. For instance, during the last glacial-interglacial cycles of the late Quaternary, a change in pCO_2 of approximately 80 – 100 ppm from glacial to interglacial periods has been documented[2], with various feedback mechanisms proposed to explain this amplitude. These mechanisms include the expansion of ice sheets[167], the higher production of corrosive Southern Component Water (SCW)[168], increased wind patterns[58,131], aeolian fertilisation and enhanced productivity in the Southern Ocean[27,132], transferring and stocking carbon in between reservoirs[124].

During the last 30,000 years (Marine Isotope Stages, MIS, 2 and 1), the Earth witnessed contrasting changes in ice volume, wind patterns, water masses geometry and ocean productivity, particularly during periods like the Last Glacial Maximum (LGM) and the last deglaciation[27,48,92,131,169]. Following these glacial conditions, the Holocene marked a shift to elevated pCO_2 levels and a decrease in Southern Ocean productivity. Previous studies for the western South Atlantic have documented enhanced primary productivity during the last glacial epoch[55,56,69,95–97], which could account for ocean carbon storage. Nevertheless, it has been proposed that biologically mediated dissolution in the South Atlantic might reduce carbon burial efficiency[33,64,65], potentially weakening the biological pump, as organic matter remineralisation corrodes carbonate. However, organic carbon and calcium carbonate accumulation rates during the last glacial continue to be high[98]. Furthermore, it has also been suggested that carbonate dissolution can respond to changes in the water masses geometry[170–172], yet its potential interaction with primary productivity and organic matter export has not been yet fully explored.

The glacial progressive replacement of Northern Component Water (NCW) by SCW at mid and greater depths of the South Atlantic Ocean has significant implications for carbonate preservation[31]. First, SCW modifies conditions for biologically mediated dissolution, notably because it contains approximately less oxygen content compared to NCW (1/3 less), which could theoretically reduce the rate of organic matter remineralisation, resulting in decreased dissolution rates. On the other hand, SCW is subsaturated in calcium carbonate, making it critical to the preservation of calcium carbonate reaching the seafloor during the last glacial epoch[31].

In this chapter, I investigate the dynamics of carbonate accumulation, focusing on key processes such as production, dilution and dissolution, during the 7 – 31 ka BP interval in the western South Atlantic. Using an integrated multi-proxy record, I show how changes in bottom water geometry affect calcium carbonate preservation at mid-depths.

Study area

The Atlantic Ocean plays an important role in the global ocean conveyor belt, distributing/transporting salt, and heat along the major ocean basins. Two of its most important characteristics are the production of deep water in the North Atlantic and the complex vertical stratification in the south[59,173]. In the South Atlantic, the circulation is dominated by two oceanographic features: the Subtropical Gyre and the Brazil-Malvinas Confluence. This confluence (at ~38°S) is the meeting point of the warm (>20°C) and salty (>36 psu) Tropical Water, that dominates the study area (**Figure 1**), transported southward in the upper layer by the Brazil Current, and the cooler (<15°C) and fresher (<34.2 psu) Malvinas Water, transported northward in the Malvinas Current[59,61].

In the southern Brazilian continental margin, below the Tropical Water, flows the South Atlantic Central Water, cooler and nutrient-rich[59], associated with a fertilisation increase in the photic zone due to upwelling events during past glacial and interglacial stages[52,105]. Below the South Atlantic Central Water, flows SCW (encompassing the Antarctic Intermediate Water, Upper Circumpolar Deep Water and Antarctic Bottom Water), promoting dissolution of calcium carbonate due to its undersaturation in carbonate ion (CO_3^{2-}). Finally, between the Upper Circumpolar Deep Water and Antarctic Bottom Water, flows southward the North Atlantic Deep Water (hereafter referred as

NCW), promoting the preservation of calcium carbonate[31]. In the past, changes in the production of both NCW and SCW have impacted the geometry and chemistry of water masses[92,174,175].

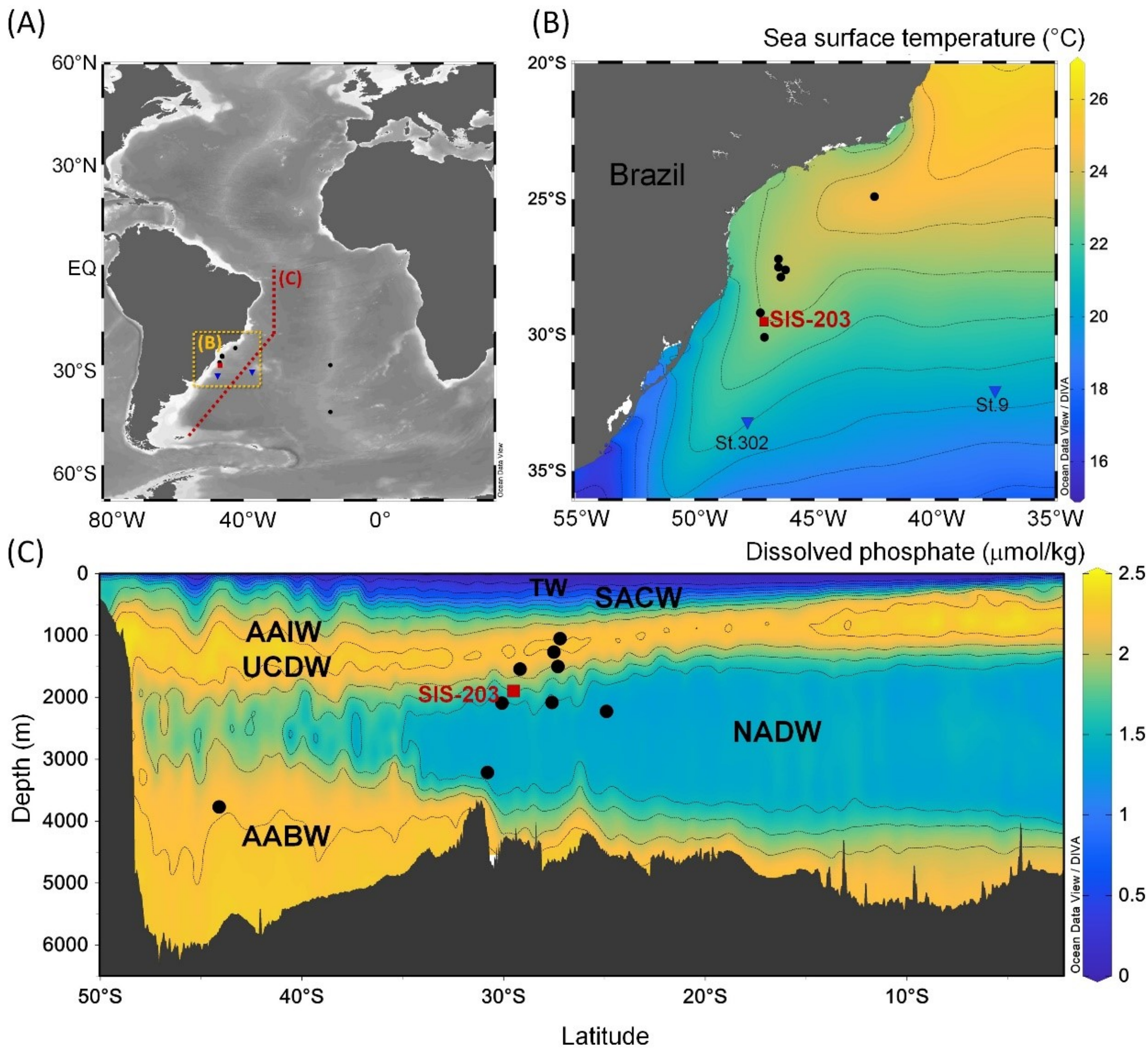

Figure 1. Location of core SIS-203, other mentioned cores (**Table 1**) and nearby seawater εNd stations[90,176] in map view (A), detailed map view with mean annual sea surface temperatures[86] (B) and latitudinal cross section using dissolved phosphate[177] (C). Water masses in C are AABW: Antarctic Bottom Water; AAIW: Antarctic Intermediate Water; NADW: North Atlantic Deep Water; SACW: South Atlantic Central Water; TW: Tropical Water; UCDW: Upper Circumpolar Deep Water. Figure made with Ocean Data View[87].

Material and methods

This study utilises sediment samples from piston core SIS-203 (3.6 m length), retrieved from the southern Brazilian continental margin at 1,894 meters below sea level (29°30′S, 47°7′W, Figure 1). Core SIS-203 was recovered during an oceanographic campaign during the austral spring-summer of 2007 by *Fugro Brasil* Ltda for the Brazilian National Agency of Petroleum, Natural Gas and Biofuels. Our results are compared to nearby cores shown in **Table 1**.

Table 1. Location details of nearby cores compared in this study.

Core	Reference	Depth (mbsl)	Latitude	Longitude
GeoB2107-3	[175]	1,050	-27.2	-46.5
KNR159-5-36	[175]	1,268	-27.5	-46.5
GeoB2104-3	[175]	1,500	-27.3	-46.4
SAT-408A	[64]	1,542	-29.1	-47.2
SIS-203	This study	1,894	-29.5	-47.1
KNR159-5-33	[174]	2,082	-27.6	-46.2
SIS-249	[65]	2,091	-30.0	-47.0
GL-1090	[174]	2,225	-24.9	-42.5
GeoB3808-6	[135]	3,213	-30.8	-14.7
MD07-3076	[178]	3,770	-44.1	-14.2

Foraminiferal analyses

To recover the planktonic foraminifera tests, each sample was washed over a 63 µm sieve, dried below 60°C and weighed. For the planktonic foraminifera assemblage compositions, 38 samples were analysed with a mean space sampling of 9 cm. Then, at least 300 non-fragmented planktonic foraminifera >150 µm were classified following the taxonomy of Brummer & Kucera[80]. To reconstruct sea surface primary productivity, we analysed the *Globigerina bulloides* and *Globigerinoides ruber* ratio *(G.bull/G.rub)*[107,179] and the relative abundance (%) of *Globigerinita glutinata*[55,107]. To assess calcium carbonate dissolution, we used the benthic planktonic foraminifera ratio (B/P)[180,181], the planktonic foraminifera fragmentation[68,182,183], the calcium carbonate content ($CaCO_3$)[184], the number of planktonic foraminifera per gram[185,186] and the ratio between fine (<63 µm) and coarse-sand (>63 µm) fraction[184,187].

Sedimentological analyses

Calcium carbonate content was measured for 67 samples by mass-loss after reaction with hydrochloric acid (HCl), 10%, at the *Centro de Geologia Costeira e Oceânica (CECO)*, *Universidade Federal do Rio Grande do Sul* (UFRGS). Grain-size analyses of 35 decarbonated samples were determined using a laser diffraction particle size analyser Horiba Partica-LA-950. Mean sortable silt was calculated as the mean size range 10 – 63 µm within the samples[188–190].

Age model

A previous age model was already published for core SIS-203[171]. Here we present an improved age model based on six published monospecific Accelerator Mass Spectrometry (AMS) radiocarbon dates combined with six new oxygen-tie correlation points (**Table 2**). All AMS radiocarbon ages were measured on planktonic foraminifera *Globigerinoides ruber* (all morphotypes) except at 21 cm, where a sample was also analysed on *Globorotalia cultrata*. We correlate the benthic $\delta^{18}O$ record[171] with the regional benthic $\delta^{18}O$ stack for intermediate depths of South Atlantic ocean (LS16-ISA)[116]. We ran the age model in the R-package "*Bacon*" v. 2.5.3, which implements Bayesian statistics[72]. We used an error of 837 years for the oxygen tie points **(Table 2)**, estimated as the geometric mean of the mean temporal resolution of core SIS-203 (351 years) and the error from the reference curve (~2000 years)[191]. The AMS radiocarbon ages were calibrated using the IntCal Marine20 curve[75], applying a local reservoir effect (deltaR) of −85 ± 40 years, based on[76–78]. For the calculation of the deltaR, we used the Marine Reservoir Correction Database (http://calib.org/marine/).

Table 2. Radiocarbon and oxygen correlation data points used for the construction of the age model for core SIS-203 on "*Bacon*" package for R software. Calibration curve number 2 corresponds to *Marine20*[75].

labID	uncalib ^{14}C age (years)	Error (years)	Depth (cm)	cc	delR	dSTD
LAC-UFF170058	6409	27	21	2	-85	40
LAC-UFF170057	7454	31	21	2	-85	40
OxygenTiePoint1	14000	837	39	0	0	0
OxygenTiePoint2	17000	837	53	0	0	0
LAC-UFF190531	13533	131	58	2	-85	40
LAC-UFF180172	15347	182	124	2	-85	40
LAC-UFF190532	18714	137	199.5	2	-85	40
LAC-UFF190533	19751	157	238.5	2	-85	40
OxygenTiePoint3	25000	837	285	0	0	0
OxygenTiePoint4	28000	837	309	0	0	0
OxygenTiePoint5	29000	837	332.5	0	0	0
OxygenTiePoint6	31500	837	375	0	0	0

Stable isotopes measurements

Oxygen ($\delta^{18}O$) and carbon ($\delta^{13}C$) stable isotope analyses were already published by Petró et al.[171], carried out on 10-15 tests of the benthic genus *Uvigerina* spp. at the Stable Isotope Laboratory of the University of California, Santa Cruz-CA (SIL-UCSC) on a dual inlet isotope ratio mass spectrometer with a Kiel IV carbonate device. Isotopic data are reported relative to the Vienna Pee-Dee Belemnite (VPDB) standard. Mean error (as 1SD) for $\delta^{18}O$ and $\delta^{13}C$ measurements is 0.05 and 0.03‰, respectively. *Uvigerina* $\delta^{18}O$ and $\delta^{13}C$ values were corrected to *Cibicidoides* using a correction of -0.47[192] and 0.90‰[193], correspondingly.

Neodymium isotopes

Neodymium isotopes analyses were carried out in uncleaned mixed planktonic foraminifera. Around 60 mg of planktonic foraminifera shells were handpicked from the >150 µm fraction, crushed and ultrasonicated to remove clays without removal of the authigenic oxides following Dias et al.[194]. The samples were then dissolved in 1 M acetic acid and centrifuged before transferred to Teflon vials. The supernatants were dried-down before re-dissolution in 0.3 M nitric acid. Rare earth elements were separated from other elements using Eichrom TRUspec™ resin and neodymium was extracted from the other REE using Eichrom Lnspec™ resin. Samples were analysed in a Thermo Neptune Plus multi-collector inductively-coupled plasma mass spectrometer (MC-ICP-MS) at the University of Cambridge (Department of Earth Sciences). Measurements were corrected for mass fractionation to a $^{146}Nd/^{144}Nd$ ratio of 0.7219. Samples were bracketed with concentration-matched solutions of standard Jndi-1[195] with a value of 0.512115±7.

Statistical analyses

We applied principal component analyses (PCA)[196] to synthesise the variation on the paleoproductivity and carbonate dissolution proxies. We used this approach as all proxies are also affected by other environmental processes[64,65]. The PCA were based on the correlation matrix of the centralised and standardised data. The normalisation was done by division of the difference between the dataset mean and the sample value by the dataset standard deviation. The synthesised productivity and dissolution proxies were extracted from the first axes of the PCAs as $PC1_P$ (productivity: *G.bull*/*G.rub* ratio and *G. glutinata* %) and $PC1_D$ (carbonate dissolution: the B/P ratio, the planktonic foraminifera fragmentation, the $CaCO_3$ %, PF/g and <63 μm/>63 μm fraction). Pearson and multiple linear correlations were conducted using the software PAST[83], version 4.05.

Results

According to our age model (**Figure 2)**, samples from core SIS-203 belong to the 31 to 7 ka BP interval and correspond to the latest Pleistocene and early/middle Holocene. The *G.bull*/*G.rub* ratio (**Figure 3**) ranges from 0.04 (at 19 ka BP) to 0.88 (at 28 ka BP) and has a mean value of 0.26 ± 0.17. The ratio shows a general and steep decreasing trend between 31 – 19 ka BP, followed by a slight increase between ~19 – 18 ka BP, and then resumes decreasing during 18 – 7 ka BP. The relative abundance of *G. glutinata* (%, **Figure 3**) varies between 7.3 (at 19 ka BP) and 20.2% (at 28 ka BP) (mean 12.5 ± 3%) and shows an overall decreasing trend except the two youngest samples (9 – 7 ka BP).

The number of planktonic foraminifera shells per gram (**Figure 3**) varies between 61 (at 17 ka BP) and 1960 (at 7 ka BP) (mean 400 ± 397), decreasing during 31 – 26 ka BP, followed by a relatively stable period (26 – 15 ka BP) and increasing towards the top (7 ka BP). The proportion of agglutinant benthic foraminifera is 0 except by the interval

21 – 15 ka BP, when it oscillates between 0 and 9%, with maximum values at 18 ka BP (**Figure 3**). The fine fraction (<63 µm/>63 µm) ranges between 9 (at 7 ka BP) and 108 (at 17 ka BP), with a mean value of 36.7 ± 21 (**Figure 3**). The calcium carbonate content ($CaCO_3$, %) benthic-planktonic foraminifera ratio (B/P) and planktonic foraminifera fragmentation proxies (**Figure 3**) were already published by Petró et al. 2021[171]. Accumulation rates were generally higher during 31 – 16 ka BP, between 15 – 23 cm/kyr, and then decreased during MIS 1 to around 3 cm/kyr (**Figure 4**). The mean sortable silt varied between 28 – 34 µm during 30 – 21 ka BP interval, then decreased to values between 19 to 29 µm along the 21 – 14 ka BP period and finally had values around 31±1 µm during the MIS 1 (**Figure 4**).

The εNd values range from -7.6 (at 22 ka BP) to -9.6 (7 ka BP), decreasing from 47 to 22 ka BP and then increasing to the top of the core. The εNd mean value is -8.66 ± 0.5 and the analytical error varied between 0.23 and 0.4 (mean 0.33 ± 0.08). Mean sortable silt ranged from 25 µm (at 19 ka BP) to 34 µm (at 29 ka BP), with a mean value of 29.6 ± 1.9 µm, during three different intervals: low values during the 21 – 14 ka BP time interval and relatively high values during 29 – 21 and 14 – 7 ka BP. Furthermore, both PCA's analyses yielded first principal components synthesising 65% of the variance on the first component (**Table 3)**.

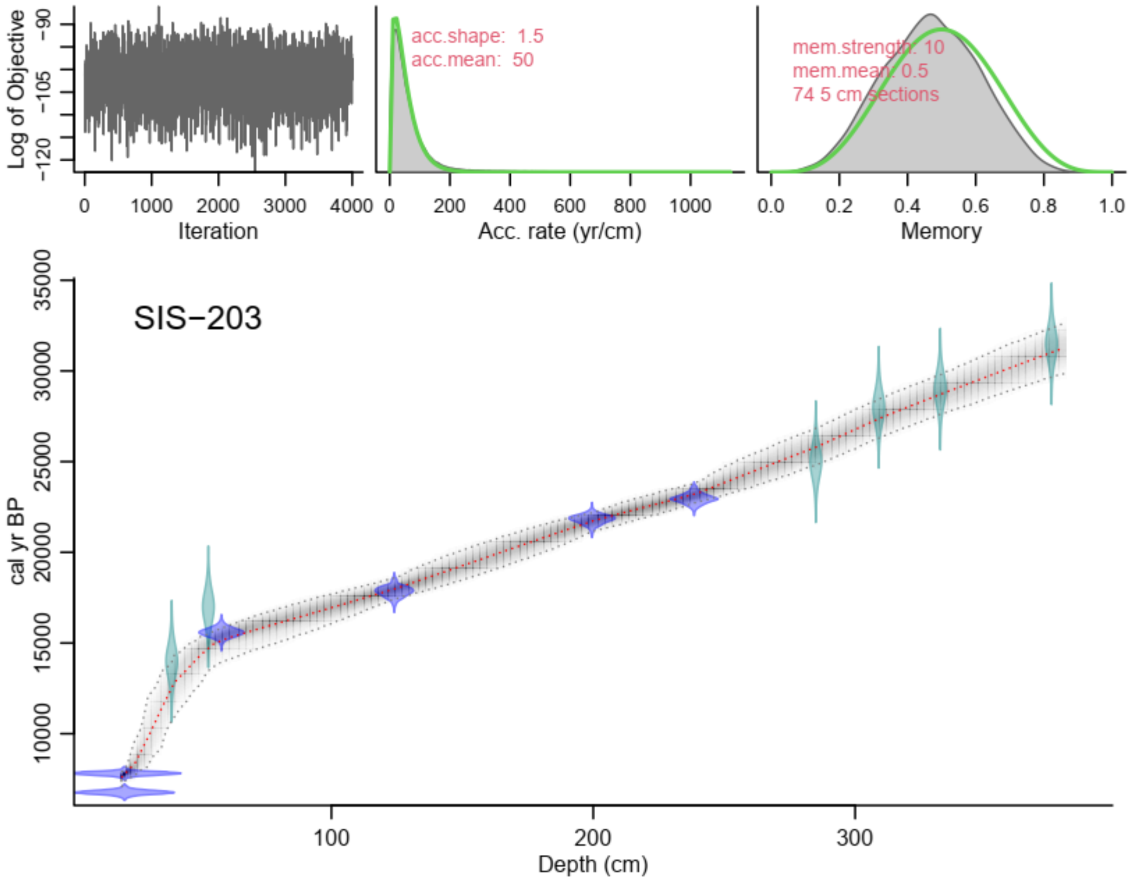

Figure 2. Age model for core SIS-203. Red dotted line shows the mean age-depth. Confidence (at 95%) is indicated by the grey envelope. Calibrated ^{14}C dates are shown in dark blue and oxygen-tie points in light blue.

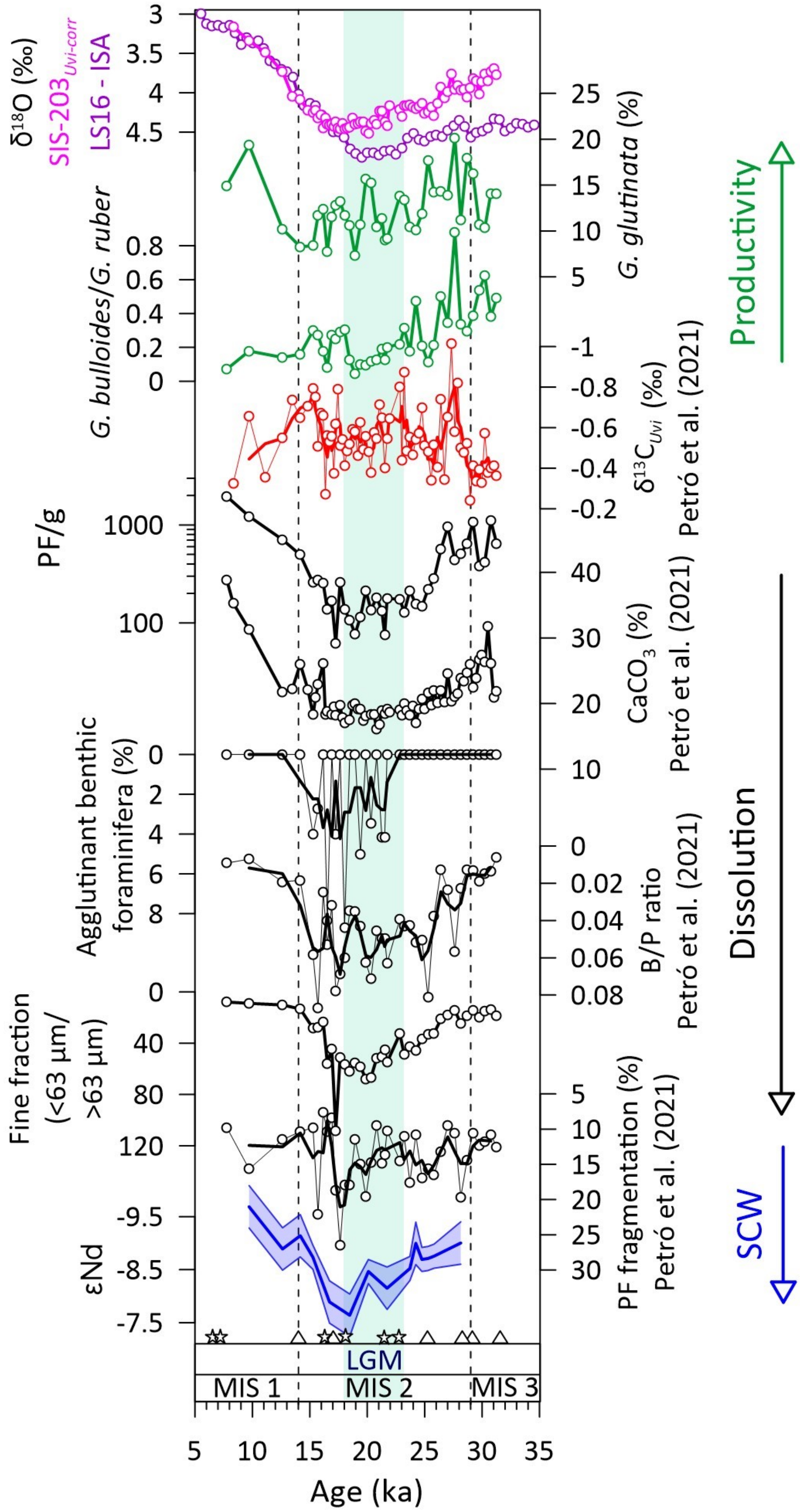

Figure 3. Time series records from core SIS-203. From top to bottom: $\delta^{18}O$ from core SIS-203 and LS16-ISA[116], *G. glutinata* abundance, *G. bulloides*/*G.ruber* ratio, $\delta^{13}C$ in *Uvigerina* spp (‰)[171], number of planktonic foraminifera per gram (PF/g), calcium

carbonate content[171] ($CaCO_3$, %), abundance of agglutinated benthic foraminifera, benthic and planktonic foraminifera ratio[171] (B/P), fine fraction (<63 µm) *vs*. sand-coarse fraction (>63 µm), fragmentation degree of planktonic foraminifera[171], and εNd from planktonic foraminiferal coatings. Error bars in εNd correspond to 2 standard deviations of reproducibility of the bracketing standards. Black vertical dashed lines divide the Marine Isotope Stages (MIS), and the blue band represents the Last Glacial Maximum (LGM). Stars represent ^{14}C dates and triangles oxygen-tie points.

Table 3. Summary of the principal component analyses for productivity and dissolution proxies.

Group	Proxy	Correlation with PC1	Variance (%)	Eigenvalue
Productivity	*G. bull* /*G. rub*	0.81	64.8	3.2
	G. glutinata (%)	0.81		
Dissolution	$CaCO_3$ (%)	-0.87	65.1	1.3
	PF/g	-0.89		
	B/P	0.84		
	<63 µm/>63 µm	0.86		
	PF fragmentation (%)	0.49		

Discussion

Age model

Although the top core ages between our model and the previously published model by Petró et al.[171] do not differ significantly, the base of core SIS-203 exhibits a significant 30 kyr off-set. The agreement at the top of the core in both models is due to calibration based on ^{14}C dates on planktonic foraminifera[197,198] (**Table 2**), a precise geochronological tool. As the off-set occurring within the 240 – 380 cm interval is based on different oxygen-tie correlation points, an additional ^{14}C date could refine the age model at the base of the core. However, due to budgetary limitations, we opted not to pursue this further analysis. Instead, we explore this difference further comparing bother age models.

Petró et al. employed AnalySeries[199], a deterministic approach that relies heavily on tie points. This method can produce less reliable models if these points are inaccurately placed, potentially leading to an over-reliance on certain tie points. On the other hand, we utilised *Bacon*[72], a Bayesian method that accounts for variability in sediment accumulation rates. The Bayesian model's adherence to realistic accumulation rates suggests a more geologically plausible scenario. In contrast, the AnalySeries model may force an unrealistic slowdown in sedimentation rates, placing the base of the core at 60 ka BP, instead of ~30 ka BP. As our oxygen-tie points align well with realistic sedimentation rates, our Bayesian age model is more robust.

While our benthic $\delta^{18}O$ stack generally aligns with the regional benthic $\delta^{18}O$ LS16-ISA stack[116] trends, there is a decoupling during the 240 – 380 cm interval, despite corrections for isotopic differences between *Uvigerina* and *Cibicidoides*. This deviation likely led Petró et al.[171] to place the base of the core at around 60 ka. Moreover, this offset also occurs the LGM, an interval based on three ^{14}C dates that align with both age models. The mismatch between our core's isotopic data and the regional reference curve can be explained from the varied water properties that compound the reference curve (0 – 35°S, 70°W – 30E), and specially the study area, located close to the southwestern boundary.

Carbonate production: surface productivity and sinking flux

To capture the processes related to carbonate dynamics over the period, we have applied a principal component analysis to summarise the variability in primary productivity and carbonate dissolution. Our first principal component of productivity proxies ($PC1_P$) suggests an enhanced glacial productivity which can be attributed to episodic upwelling events during late MIS 3 and early MIS 2 (**Figure 3**, *G. bulloides*/*G. ruber* ratio), in agreement with previous studies for the southern Brazilian continental margin[55,56,96,200]. A decrease in the $PC1_P$ is observed towards the deglaciation, with a slight increase during the Holocene, due to the relatively high abundance of *Globigerinita glutinata* (%).

Previous studies suggested a biologically mediated carbonate dissolution[33,34] for the study area during MIS 2 – 4[64,65]. This process occurs due to the remineralisation of labile organic carbon fixed by phytoplankton during glacial upwelling events[70,97], leading to release of CO_2 and decrease of pH. However, in our record $PC1_P$ and $PC1_D$ are not positively correlated. Instead, a weak and negative (linear) correlation between $PC1_P$ and $PC1_D$ is observed (**Figure 4,** R = -0.32, *p*-value = 0.04), suggesting that carbonate accumulation at the seafloor could be a direct result of the sinking flux of particles from the surface. Yet, since the correlation value is rather low and productivity was documented to be low during the Holocene for the southern Brazilian continental margin[55,69], it is very likely that other parameters (also) controlled the carbonate accumulation dynamics.

For instance, similar variations between $PC1_D$ (first principal component of dissolution proxies) and accumulation rates (**Figure 4**, R = 0.66 *p*-value<0.01) could suggest a dilution effect on the carbonate content (**Figure 4**) due to the elevated particle fluxes. If vertical particle fluxes increased due to a boosted biological pump, both elevated burial rates and decrease exposure to the seafloor dynamics should preserve the carbonate. But the benthic planktonic foraminifera (B/P) ratio and the planktonic foraminifera fragmentation (PF fragmentation) index point to elevated carbonate dissolution in times of high accumulation rates, suggesting that indeed calcium carbonate was not effectively preserved.

Although sinking velocities of planktonic foraminifers through the water column are relatively fast[201], an important part of the biogenic carbonate produced at the surface ocean is dissolved before reaching the deep sea-floor[35,202]. This loss has been related to two processes: metabolic processes and high magnesium calcites for shallow-water dissolution, and solubility of $CaCO_3$ for deeper waters[30]. As the first process involves biogeochemical relations[203,204] out of the scope of this paper, we focus on the influence of chemical properties of the overlaying water masses in the next section.

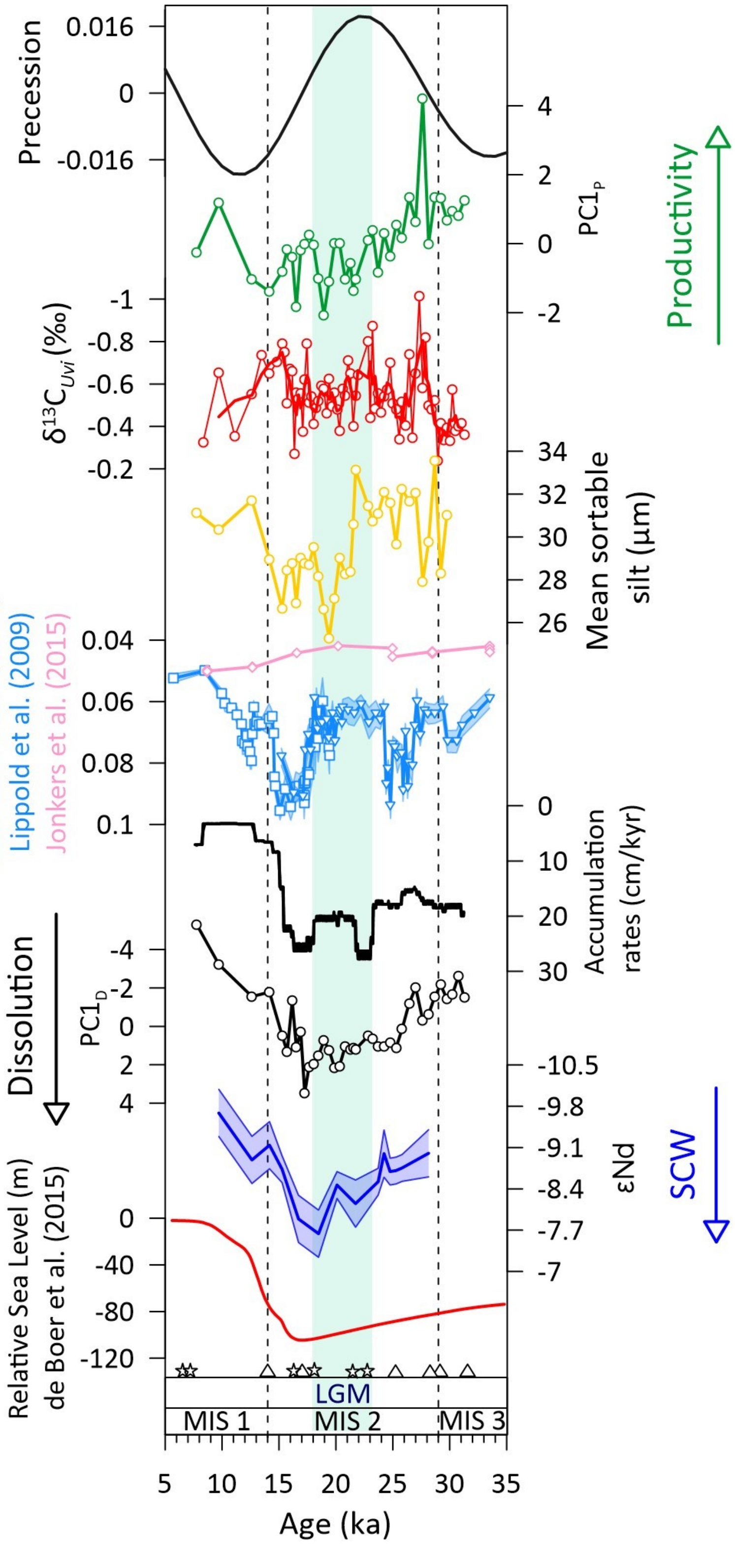

Figure 4. Time series records of paleoproductivity, dissolution and water masses influence among other proxies. From top to bottom: precession values[123], synthesised records of productivity ($PC1_P$), infaunal $\delta^{13}C$ from *Uvigerina* spp (‰), mean sortable silt (µm), $^{231}Pa/^{230}Th$ records from the Atlantic Ocean[135,205,206], accumulation rates (cm/kyr),

synthesised records of dissolution ($PC1_D$), εNd from planktonic foraminiferal coatings and relative sea level[207]. Error bars in εNd correspond to 2 standard deviations of reproducibility of the bracketing standards. The black vertical dotted lines divide the Marine Isotope Stages (MIS), while the blue band represents the Last Glacial Maximum. Stars represent ^{14}C dates and triangles oxygen-tie points.

Carbonate dissolution: water mass geometry and bottom currents

Distinct stratification patterns, produced by changes in the water mass geometry during distinct climate stages, redistribute the organic and inorganic carbon within the major ocean basins[92,168]. With different carbonate ion saturation states, the relative replacement of NCW by SCW has the potential to dissolve biogenic carbonate that reach the seafloor[137,208], being suggested that higher proportions of SCW were the cause of carbonate dissolution at the study site[171]. Being controlled by biological processes at both surface (photosynthesis) and deep (remineralisation) oceans, benthic $\delta^{13}C$ has been historically utilised to reconstruct water masses mixing[209–212]. While a broader shift in benthic $\delta^{13}C$ values from core SIS-203 is expected due to the NCW and SCW production dynamics, **Figure 4** displays a relative stability, particularly when compared with the Holocene vertical benthic $\delta^{13}C$ profile (**Figure 5**). This lack of variation could be attributed to the use of the genus *Uvigerina*, an infaunal benthic foraminifera that dwells within the sediment[193], being more probably influenced by pore water chemistry and/or productivity rather than bottom water mass characteristics[193,213,214].

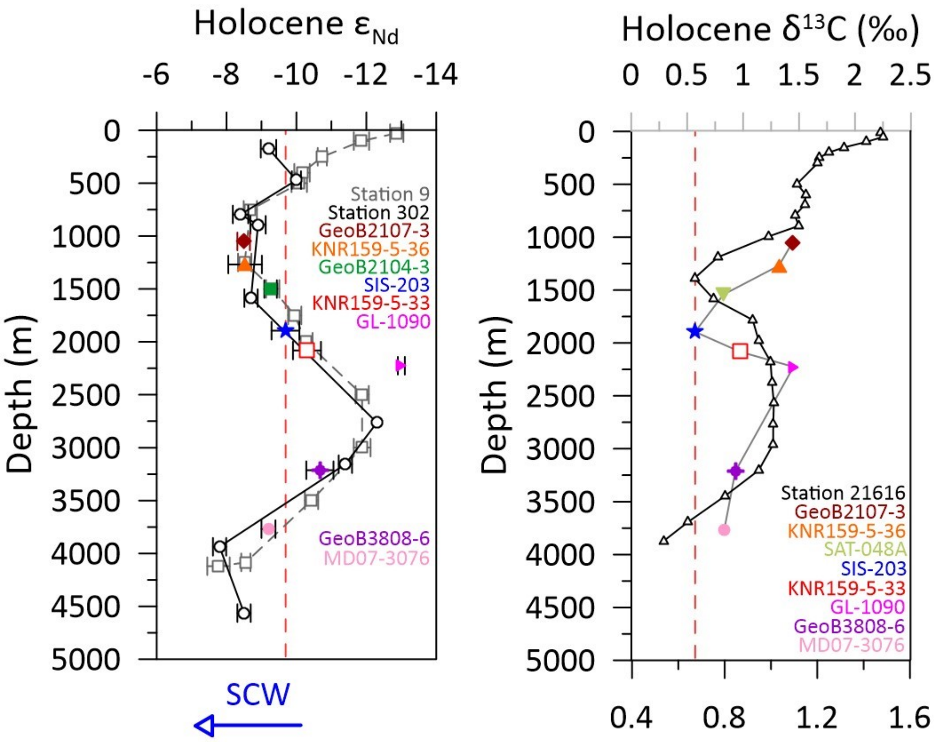

Figure 5. Holocene εNd and $\delta^{13}C$ values from core SIS-203 (this study), nearby stations 9[90], 302[69] and 21616[215] and core tops (GeoB2107-3, KNR159-5-36, GeoB2104-3[175,216]; KNR159-5-33, GL-1090[174,217]; GeoB3808-6[135] and MD07-3076[178,218]). Vertical dashed lines locate measurements from core SIS-203 on each graph.

However, previous studies have shown that both epifaunal (e.g., *Cibicidoides*) and infaunal (e.g., *Uvigerina*) benthic foraminifera can record changes in $\delta^{13}C$ during the last deglacial[178,218], suggesting that our *Uvigerina* $\delta^{13}C$ values can indeed reflect broader water mass signals. Thus, it might be that our *Uvigerina* $\delta^{13}C$ values capture a rather stable carbon isotopic signature of the bottom water, very likely because the coring site falls within a zone where the interplay between NCW and SCW, and the variation of the end-members values during glacial-interglacial dynamics, results in a relatively stable $\delta^{13}C$ signal, despite the changes in the water masses geometry. Furthermore, $\delta^{13}C$ measurements from shallower sites (GeoB2107-3[175], KNR159-5-36[216], SAT-048A[69]) and deeper than core SIS-203 (KNR159-5-33[174], GL-1090[217], GeoB3808-6[135]) presented more negative $\delta^{13}C$ values during the LGM, indicating an accumulation of respired carbon on the water column from 1000 to ~3500 m depth.

To accurately assess the potential of water mass geometry changes on carbonate dynamics at our site, we reconstructed the authigenic εNd from core SIS-203. Neodymium isotopes serve as valuable tracers for water masses because they carry characteristic signatures based on their formation regions. Seawater εNd is influenced by water mass provenance and the mixing proportions, once it is not significantly fractionated by marine biological processes[91,219–222]. The authigenic εNd measured in foraminiferal coatings from our core top sample (-9.69±0.04) aligns well with modern seawater εNd (-9.95±0.19) from nearby Station 9[90]. Although measurements from Station 302[176] are from different depths, our foraminiferal εNd values fall right in between the upper and lower points (**Figure 5**). Our core top measurement also corresponds closely with the Holocene foraminiferal εNd profile, based on nearby sediment cores GeoB2107-3, KNR159-5-36, GeoB2104-3[175]; KNR159-5-33 and GL-1090[174]. Cores GeoB3808-6[135] and MD07-3076[178] (**Figure 5, Table 1**), located in the mid-Atlantic Ridge, also align with the modern seawater and Holocene authigenic εNd vertical profiles. The agreement between the SIS-203 core top to the seawater and nearby εNd core tops suggests that the foraminiferal εNd values in our study area faithfully reflect the past seawater εNd conditions rather than being influenced by local Nd sources[223].

However, as end-member values have varied over time[224,225], converting εNd values to proportions of ancient Northern Component Water (NCW) *vs*. Southern Component Water (SCW), specific end-member values should be utilised[224]. Using the equation presented by Howe et al.[92] (**see methods**), we estimated NCW/SCW proportions for two samples: core top and Last Glacial Maximum (LGM). For the core top analysis, we employed $\delta^{13}C$ and εNd values from Perez-Asensio et al.[226] for the North Atlantic Deep Water (NADW), considered here as NCW, and Circumpolar Deep Water (CDW) as SCW. The results indicate that NCW constituted approximately 45±9% of the water mass at the core top. For the LGM, we used $\delta^{13}C$ and εNd values from Yu et al.[138] for the Glacial North Atlantic Intermediate Water (GNAIW, as NCW,) and Glacial Antarctic Bottom Water (GAABW, as SCW). Here, the LGM sample showed a reduced NCW influence, down to 23±9%. (**Figure 6**). Without incorporating end-member variability, the εNd values from the LGM would falsely imply a total absence of NCW (0%), leading to assumptions of a complete cessation of NCW influence, a scenario similar to reconstructions based on benthic $\delta^{13}C$[211,212].

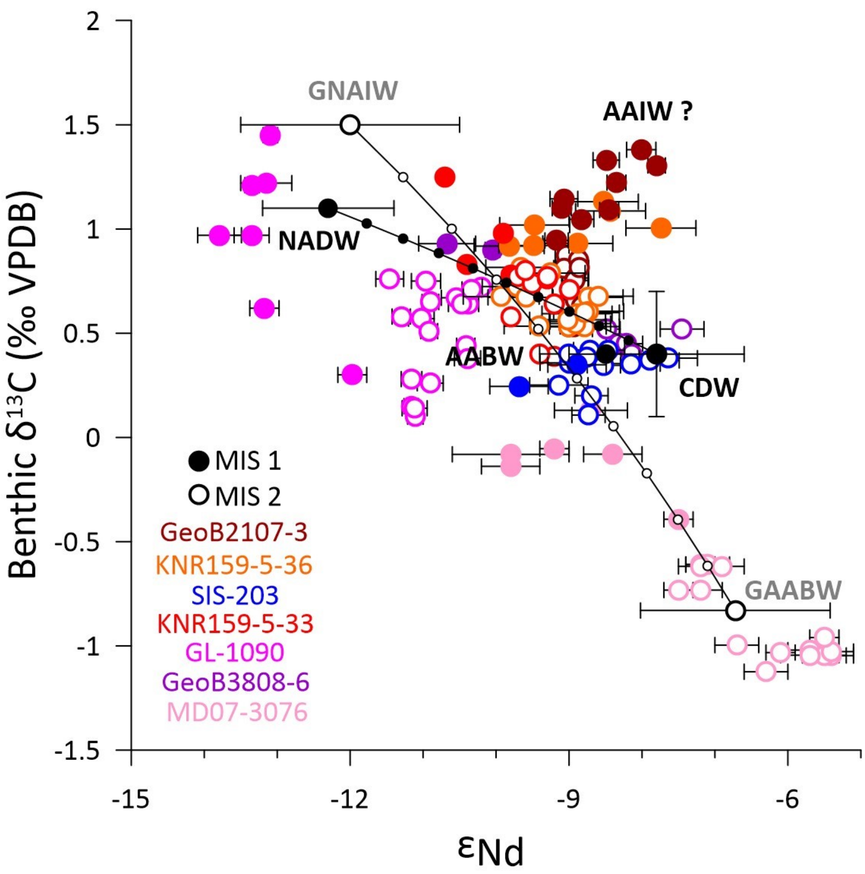

Figure 6. Benthic δ13C *vs*. foraminiferal εNd from cores SIS-203 (this study), GeoB2107-3, KNR159-5-36, GeoB2104-3[175,216]; KNR159-5-33, GL-1090[92,217] and MD07-3076[178,218]. εNd analyses in GeoB3808-6 were carried out in bulk sediment[135]. Open (filled) circles belong to marine isotope stage, MIS, 1 (2). The black (white) dots-line represents the binary mixing model for nowadays (last glacial maximum) NADW (GNAIW) and CDW (GAABW) end-members, as NCW and SCW respectively (**see discussion**).

Furthermore, our foraminiferal εNd revealed that larger proportions of the more corrosive SCW (22±9%) bathed our coring site during the LGM and Heinrich Stadial 1 (**figures 4 and 6**). In our scenario, $PC1_D$ is higher when foraminiferal ε_{Nd} values are more radiogenic (more SCW). As our core SIS-203 is in the interphase between SCW and NCW mixing, our multi-proxy study suggests that the changes in the water masses geometry predominantly affected the carbonate preservation, being responsible for the fragmentation of planktonic foraminifera, relative increase in benthic foraminifera (up to 8%) and the higher presence of agglutinated benthic foraminifera. Moreover, the relative replacement of NCW by SCW could also impact the carbonate preservation by slower bottom current velocities which could lead to the accumulation of respired CO_2, a subsequent reduction in pH, and then to carbonate dissolution. This phenomenon is supported by our mean sortable silt measurements (**Figure 4**). Moreover, although a reduction in the strength of the Atlantic Meridional Overturning Circulation during the Heinrich Stadial 1 (based on $^{231}Pa/^{230}Th$ values from the Bermuda Rise[205]) is concomitant with our maximum values of $PC1_D$, this is not the case for the Heinrich Stadial 1. Furthermore, $^{231}Pa/^{230}Th$ values from the mid-Atlantic ridge (GeoB3808-6[135]) show no variations (**Figure 4,** in pink). Yet, discussing the influence of millennial-scale variability with our proxy records is complicated due to the temporal resolution of our proxy, especially our foraminiferal εNd.

Carbon reservoir effectiveness During Glacial Periods

The here documented SCW-related dissolution (at ~1,900 m depth, core SIS-203) and biologically mediated dissolution (at ~1,500 and 2,100 m depths[64,65]) in the western South Atlantic mirror parallel processes for the eastern South Atlantic[122]. Despite utilising different methodologies (i.e., productivity measured as accumulation rates of total organic carbon and dissolution as sand content) and deeper cores (between ~2,500 – 4,700 m depth), the authors[122] also recognised both water masses and productivity as triggers of carbonate dissolution, proving the extensive impact of these factors across the South Atlantic. Interestingly, the inverse effect of productivity in preserving carbonate is more notable in equatorial cores within the upwelling zone (both now and in glacial times).

Building on this, the detection of a consistent 23-kyr cycle in biologically mediated dissolution patterns across the Indian Ocean[33] and the eastern South Atlantic[122], suggests a strong climatic control within major ocean basins. For the western South Atlantic, this precessional forcing has been suggested[64], although longer temporal records are necessary to further prove this orbital influence. These cyclical patterns, indicative of the Earth's precessional cycle, shows how primary productivity and subsequent organic matter degradation directly influence carbonate dissolution rates, offering insights into the past dynamics that may inform future climatic projections. Furthermore, understanding the physicochemical properties and dynamics of SCW and NCW during glacial periods is crucial for understanding the ocean's role as a carbon reservoir.

Both, elevated primary productivity and SCW production significantly influences the calcium carbonate dynamics, which in turn affects the Earth's climate system through feedback mechanisms. During glacial periods, elevated productivity enhances the flux of organic matter to the seafloor, which is, in part, effectively buried[98]. This increased organic matter flux, coupled with biologically mediated dissolution, contributes to the deep ocean's role as an effective carbon reservoir. The remineralisation of labile organic leads to the release of CO_2 and a decrease in pH, further enhancing carbonate dissolution. On top of it, SCW's corrosive nature significantly impacts carbonate records by promoting dissolution of carbonate sediments. Yet, carbonate dissolution buffers the oceans, which increases their alkalinity and ability to store more carbon during glacial times[24,168,227].

The here documented carbonate (and carbon) dynamics, despite dissolution (and remineralisation), makes the western south Atlantic an effective carbon reservoir/sequestration through enhanced productivity and carbonate dynamics. Understanding these interactions is crucial for refining current climatic models, which, in turn, could better project future states of the global climate system.

Conclusion

Our analysis of productivity proxies ($PC1_P$) reveals increased productivity mainly during MIS 2. For the Holocene, high values of *Globigerinita glutinata* (%) increases the $PC1_P$, contrary to previous studies in the area. Negatively correlated with the $PC1_P$, our dissolution proxies ($PC1_D$) indicate that surface particle flux contributes to carbonate accumulation, though other factors are at play. Based on authigenic εNd analyses, we hypothesise that the expansion of Southern Component Water (SCW) during the Last Glacial Maximum had a significant impact on the carbonate dissolution. Although reduced oxygen content in SCW could potentially preserve organic matter by limiting remineralisation, the labile nature of glacial organic matter and slower bottom current velocities likely led to increased respired CO_2 accumulation, reduced pH, and then enhancing carbonate dissolution.

During glacial periods, increased productivity and biologically mediated dissolution enhance the ocean's role as an effective carbon reservoir. The western South Atlantic demonstrates significant carbon sequestration through boosted productivity and carbonate dynamics, highlighting the importance of this oceanographical setting in the global carbon cycle. Future research should constrain in time, space, magnitude and nature the high productive events on southern Brazilian continental margin, as well as their impact in carbon and carbonate burial at different sea depths. This understanding is crucial to improve our knowledge of past and future climate dynamics, particularly regarding the ocean's capacity for carbon sequestration.

Chapter 6: Conclusions

✓ **Differential Fertilisation Mechanisms**:

The southern and southeast Brazilian continental margins seem to be influenced by different fertilisation mechanisms during the MIS 5 – 1 time interval. The southeast region is more likely affected by eccentricity-paced mechanisms, while the southernmost margin might be influenced by Antarctic ice sheet dynamics. Proximity to the coastline also plays a crucial role, as continental (terrigenous or riverine) fertilisation can impact sea surface primary productivity.

✓ **Carbonate Dissolution and Burial**:

Mid-Depths (~1,500 mbsl): High productivity at mid-depths can lead to carbonate dissolution, as evidenced in the western, eastern Atlantic, and Indian Oceans. This biologically mediated dissolution affects carbonate burial rates. Although carbonate is dissolved and re-enters the system, overall accumulation rates are higher, effectively sequestering carbon in both seafloor water and sediments during high productivity intervals.

Greater Depths (~2,000 mbsl): At greater depths, carbonate dissolution is driven by the carbonate ion saturation state, linked to glacial-interglacial changes likely associated with Antarctic ice sheet development and bottom water masses geometry. These changes influence physical and biogeochemical processes, impacting CO_2 levels. However, longer time interval records are needed to confirm this.

✓ **Dissolution Imprint in Planktonic Foraminiferal Tests**:

The dissolution imprint in planktonic foraminiferal test sizes can be subtle but significant, potentially affecting other proxies used in palaeoclimatic reconstructions. Dissolution can alter the chemical and isotopic composition of foraminiferal tests, which may lead to misinterpretations of past oceanic conditions. Recognising and accounting for these subtle dissolution imprints is essential for improving the accuracy of palaeoenvironmental proxies.

Although insolation-related enhanced biological pump can sequester carbon in the sediments in the study area, enhanced southern component water production and subantarctic biological pump during glacial periods, related to Antarctic ice sheet and south westerly winds dynamics, play a more relevant role in controlling CO_2 levels and carbonate accumulation. Current global warming and the deterioration of Antarctic systems can potentially affect the southernmost Brazilian margin through the links here explored. The changes in wind patterns and ocean currents influenced by Antarctic ice dynamics can have downstream effects on productivity and carbon cycling in this region, affecting the ocean's capacity to effectively sequester carbon.

Chapter 7:
Future Research

Building on the findings from this study, future research should aim to investigate longer temporal sediment cores, specifically reaching MIS 6 – 5, to examine how the southernmost Brazilian continental margin responded to past climate changes in terms of productivity, organic matter export, and carbonate dissolution. This could provide a clearer understanding of how these processes evolved over time and their potential impact on the global carbon cycle.

Further research is needed to explore the role of fluvial and terrestrial fertilisation mechanisms in the southwestern Atlantic, particularly their influence on productivity in both coastal and open ocean settings. This could help clarify the interactions between terrestrial inputs and marine processes observed in this study.

Additionally, more complete records are required to assess the influence of orbital cyclicity (precession and obliquity) on productivity and dissolution patterns, which were here highlighted as key factors. Understanding these cycles in greater detail will contribute to a better understanding of how they drive regional and global climatic changes.

Investigating the total organic carbon in the sediments could further elucidate the mechanisms behind carbon export from enhanced primary productivity, a process suggested to be critical for carbon sequestration in the region.

Moreover, examining how the southwestern Atlantic responded to changes in Antarctic ice sheets (both in terms of timing and impact) will be crucial in understanding the region's role in global climate dynamics. This because of the observation of latitudinal variations in productivity and carbonate dissolution linked to high southern latitude processes.

Further research should also investigate the geometry of water masses during the last interglacial epoch and its relationship with Antarctic ice sheets, carbonate dissolution in deep waters and even mid-depths. This could shed light on the interactions between water masses and carbonate chemistry.

Finally, future studies should focus on characterising the variations in the size of fragments and broken planktonic foraminifera. By removing taphonomic effects and reconstructing ecological signals, these studies could refine our understanding of the environmental conditions during the periods studied.

References

1. Riebesell, U. Effects of CO2 Enrichment on Marine Phytoplankton. *J. Oceanogr.* **60**, 719–729 (2004).

2. Petit, J. R. *et al.* Climate and atmospheric history of the past 420,000 years from the Vostok ice core, Antarctica. *Nature* **399**, 429–436 (1999).

3. Martínez-Botí, M. A. *et al.* Plio-Pleistocene climate sensitivity evaluated using high-resolution CO2 records. *Nature* **518**, 49–54 (2015).

4. de la Vega, E., Chalk, T. B., Wilson, P. A., Bysani, R. P. & Foster, G. L. Atmospheric CO2 during the Mid-Piacenzian Warm Period and the M2 glaciation. *Sci. Rep.* **10**, 14–21 (2020).

5. IPCC. Summary for Policymakers. Climate Change 2021: The Physical Science Basis. 41 (2021).

6. Van de Waal, D. B., John, U., Ziveri, P., Reichart, G. & Hoins, M. Ocean Acidification Reduces Growth and Calcification in a Marine Dinoflagellate. *PLoS One* **8**, e65987 (2013).

7. Orr, J. C. *et al.* Anthropogenic ocean acidification over the twenty-first century and its impact on calcifying organisms. *Nature* **437**, 681–686 (2005).

8. Parmesan, C. & Yohe, G. A globally coherent fingerprint of climate change impacts across natural systems. *Nature* **421**, 37–42 (2003).

9. Poloczanska, E. S. *et al.* Global imprint of climate change on marine life. *Nat. Clim. Chang.* **3**, 919–925 (2013).

10. Terry L. Root *et al.* Fingerprints of global warming on wild animals and plants. *Nature* **421**, 54–57 (2003).

11. Frölicher, T. L., Fischer, E. M. & Gruber, N. Marine heatwaves under global warming. *Nature* **560**, 360–364 (2018).

12. Schiermeier, Q. Clear signs of global warming will hit poorer countries first news. *Nature* **556**, 415–416 (2018).

13. van Daalen, K. R. *et al.* The 2024 Europe report of the Lancet Countdown on health and climate change: unprecedented warming demands unprecedented action. *Lancet Public Heal.* **9**, e495–e522 (2024).

14. Cai, W. *et al.* Increased frequency of extreme Indian ocean dipole events due to greenhouse warming. *Nature* **510**, 254–258 (2014).

15. Shackleton, N. J. Oxygen isotopes, ice volume and sea level. *Quat. Sci. Rev.* **6**, 183–190 (1987).

16. Imbrie, J. *et al.* On the structure and origin of major glaciation cycles 1. Linear responses to Milankovitch forcing. *Paleoceanography* **7**, 701–738 (1992).

17. Jouzel, J. *et al.* Orbital and Millennial Antarctic Climate Variability over the Past. *Science (80-.).* **317**, 793–796 (2007).

18. Parrenin, F. *et al.* Synchronous Change of Atmospheric CO2 and Antarctic Temperature During the Last Deglacial Warming. *Science (80-.).* **339**, (2013).

19. Milankovitch, M. Kanon der Erdbestrahlungen und seine Anwendung auf das Eiszeitenproblem. *R. Serbian Acad. Sect. Math. Nat. Sciecnes* **33**, (1941).

20. Berger, A. Milankovitch theory and climate. *Rev. Geophys.* **26**, 624–657 (1988).

21. Hays, J. D., Imbrie, J. & Shackleton, N. J. Variations in the earth's orbit: Pacemaker of the ice ages. *Science (80-.).* **194**, 1121–1132 (1976).

22. Huybers, P. Early Pleistocene Glacial Cycles and the Integrated Summer. *Science (80-.).* **313**, 508–511 (2006).

23. Sigman, D. M. & Boyle, E. A. Glacial/Interglacial changes in atmospheric carbon dioxide. *Nature* **407**, 859–869 (2000).

24. Sigman, D. M., Hain, M. P. & Haug, G. H. The polar ocean and glacial cycles in

atmospheric CO2 concentration. *Nature* **466**, 47–55 (2010).

25. Ai, X. E. *et al.* Southern Ocean upwelling, Earth's obliquity, and glacial-interglacial atmospheric CO2 change. *Science (80-.).* 1348–1352 (2021).

26. Devries, T., Primeau, F. & Deutsch, C. The sequestration efficiency of the biological pump. *Geophys. Res. Lett.* **39**, 1–5 (2012).

27. Martínez-Garcia, A. *et al.* Links between iron supply, marine productivity, sea surface temperature, and CO2 over the last 1.1 Ma. *Paleoceanography* **24**, 1–14 (2009).

28. Martínez-García, A. *et al.* Iron fertilization of the subantarctic ocean during the last ice age. *Science (80-.).* **343**, 1347–1350 (2014).

29. Schiebel, R. Planktic foraminiferal sedimentation and the marine calcite budget. *Global Biogeochem. Cycles* **16**, 1–21 (2002).

30. Sulpis, O., Jeansson, E., Dinauer, A., Lauvset, S. K. & Middelburg, J. J. Calcium carbonate dissolution patterns in the ocean. *Nat. Geosci.* **14**, 423–428 (2021).

31. Frenz, M., Hoppner, R., Stuut, J.-B., Wagner, T. & Henrich, R. Surface sediment bulk geochemistry and grain-size composition related to the oceanic circulation along the south american continental margin in the southwest atlantic. in *The South Atlantic in the Late Quaternary* (eds. Wefer, G., Mulitza, S. & Ratmeyer, V.) 347–373 (Berlin, Heidelberg, New York, Tokyo: Springer-Verlag, 2003). doi:10.1007/978-3-642-18917-3_17

32. Wagner, T. Control of organic carbon accumulation in the late Quaternary equatorial Atlantic (Ocean Drilling Program sites 664 and 663): Productivity versus terrigenous supply. *Paleoceanography* **15**, 181–199 (2000).

33. Schulte, S. & Bard, E. Past changes in biologically mediated dissolution of calcite above the chemical lysocline recorded in Indian Ocean sediments. *Quat. Sci. Rev.* **22**, 1757–1770 (2003).

34. Milliman, J. D. *et al.* Biologically mediated dissolution of calcium carbonate above the chemical lysocline ? *Deep. Res. Part I* **46**, 1653–1669 (1999).

35. Petró, S. M., Do Nascimento Ritter, M., Pivel, M. A. G. & Coimbra, J. C. Surviving in the water column: Defining the taphonomically active zone in pelagic systems. *Palaios* **33**, 85–93 (2018).

36. Huybers, P. & Wunsch, C. Obliquity pacing of the glacial cycles. *Nature* **414**, 491–494 (2005).

37. Huybers, P. Glacial variability over the last two million years: an extended depth-derived agemodel, continuous obliquity pacing, and the Pleistocene progression. *Quat. Sci. Rev.* **26**, 37–55 (2007).

38. Watanabe, Y. *et al.* Astronomical forcing shaped the timing of early Pleistocene glacial cycles. *Commun. Earth Environ.* **4**, 1–11 (2023).

39. Paillard, D. Climate and astronomical cycles. in *Paleoclimatology* (ed. Ramstein, G.) (Springer Nature, 2021). doi:10.1007/978-3-030-24982-3_28

40. Chiang, J. C. H. & Bitz, C. M. Influence of high latitude ice cover on the marine Intertropical Convergence Zone. *Clim. Dyn.* **25**, 477–496 (2005).

41. Marino, G. *et al.* Agulhas salt-leakage oscillations during abrupt climate changes of the Late Pleistocene. *Paleoceanography* **28**, 599–606 (2013).

42. Govin, A. *et al.* Evidence for northward expansion of Antarctic Bottom Water mass in the Southern Ocean during the last glacial inception. *Paleoceanography* **24**, 1–14 (2009).

43. Stephens, B. B. & Keeling, R. F. The influence of antarctic sea ice on glacial-interglacial CO2 variations. *Nature* **404**, 171–174 (2000).

44. Gottschalk, J. *et al.* Biological and physical controls in the Southern Ocean on past millennial-scale atmospheric CO2 changes. *Nat. Commun.* **7**, (2016).

45. Teitler, L. *et al.* Determination of Antarctic Ice Sheet stability over the last ~500

ka through a study of iceberg-rafted debris. *Paleoceanography* **25**, 1–18 (2010).

46. Kanfoush, S. L., Hodell, D. A., Charles, C. D., Janecek, T. R. & Rack, F. R. Comparison of ice-rafted debris and physical properties in ODP Site 1094 (South Atlantic) with the Vostok ice core over the last four climatic cycles. *Palaeogeogr. Palaeoclimatol. Palaeoecol.* **182**, 329–349 (2002).

47. Barkley, A. E. *et al.* Patagonian dust, Agulhas Current , and Antarctic ice-rafted debris contributions to the South Atlantic Ocean over the past 150,000 years. *Proc. Natl. Acad. Sci.* **120**, 2017 (2024).

48. Lisiecki, L. E. & Raymo, M. E. A Pliocene-Pleistocene stack of 57 globally distributed benthic d18O records. *Paleoceanography* **20**, 1–17 (2005).

49. Portilho-ramos, C., Ferreira, F., Calado, L., Frontalini, F. & de Toledo, M. B. Variability of the upwelling system in the southeastern Brazilian margin for the last 110,000 years. *Glob. Planet. Change* **135**, 179–189 (2015).

50. Petró, S. M., Maria, A. N. A. & Mizusaki, P. PALEOCEANOGRAPHIC CHANGES THROUGH THE LAST 130 KA IN THE WESTERN SOUTH ATLANTIC BASED. **19**, 3–14 (2016).

51. Lessa, D. V. O., Santos, T. P., Venancio, I. M., Luiza, A. & Albuquerque, S. Offshore expansion of the Brazilian coastal upwelling zones during Marine Isotope Stage 5 O ff shore expansion of the Brazilian coastal upwelling zones during Marine Isotope Stage 5. *Glob. Planet. Change* **158**, 13–20 (2017).

52. Lessa, D. V. O. *et al.* Eccentricity-induced expansions of Brazilian coastal upwelling zones. *Glob. Planet. Change* **179**, 33–42 (2019).

53. Naidu, P. D. & Malmgren, B. A. Monsoon upwelling effects on test size of some planktonic foraminiferal species from the Oman Margin, Arabian Sea. *Paleoceanography* **10**, 117–122 (1995).

54. Conan, S. M. & Brummer, G. A. Fluxes of planktic foraminifera in response to monsoonal upwelling on the Somalia Basin margin. **47**, 2207–2227 (2000).

55. Pereira, L. S., Arz, H. W., Patzold, J. & Portilho-Ramos, R. D. C. Productivity Evolution in the South Brazilian Bight During the Last 40 , 000 Years Paleoceanography and Paleoclimatology. *Paleoceanogr. Paleoclimatology* **33**, 1–18 (2018).

56. Portilho-ramos, R. C. *et al.* Understanding the mechanisms behind high glacial productivity in the southern Brazilian margin. *Clim. Past* **15**, 943–955 (2019).

57. Lopes, R. P. *et al.* Late Pleistocene sediment accumulation in the lower slope off the Rio Grande terrace, southern Brazilian Continental Margin. *Quat. Int.* **571**, 97–116 (2021).

58. Toggweiler, J. R., Russell, J. L. & Carson, S. R. Midlatitude westerlies , atmospheric CO2, and climate change during the ice ages. *Paleoceanography* **21**, 1–15 (2006).

59. Piola, A. R. & Matano, R. P. Ocean Currents: Atlantic Western Boundary—Brazil Current/Falkland (Malvinas) Current. *Ref. Modul. Earth Syst. Environ. Sci.* **3**, 414–420 (2019).

60. Matano, R. P., Palma, E. D. & Piola, A. The influence of the Brazil and Malvinas Currents on the Southwestern The influence of the Brazil and Malvinas Currents on the Southwestern Atlantic Shelf circulation. *Ocean Sci.* **6**, 983–995 (2010).

61. Peterson, R. G. & Stramma, L. Upper-level circulation in the South Atlantic Ocean. *Prog. Ocean.* **26**, 1–73 (1991).

62. Piola, A. R., Matano, R. P., Palma, E. D. & Mo, O. O. The influence of the Plata River discharge on the western South Atlantic shelf. **32**, 4–7 (2005).

63. Pimenta, F. M. *et al.* A NUMERICAL STUDY OF THE PLATA RIVER PLUME ALONG THE SOUTHEASTERN SOUTH AMERICAN CONTINENTAL SHELF. **53**, 129–146 (2005).

64. Suárez-Ibarra, J. Y. *et al.* Calcium Carbonate Dissolution Triggered by High Productivity During the Last Glacial–Interglacial Interval in the Deep Western

South Atlantic. *Front. Earth Sci.* **10**, 1–14 (2022).

65. Suárez-Ibarra, J. Y. *et al.* Surface fertilisation and organic matter delivery enhanced carbonate dissolution in the western South Atlantic. *Front. Ecol. Evol.* **11**, 1–14 (2023).

66. Suárez-Ibarra, J. Y. *et al.* PLANKTONIC FORAMINIFERA TEST SIZE DICTATED BY CONDITIONS IN LIFE AND POST-MORTEM [Pre-print]. *AUTHOREA* (2024). doi:10.22541/au.171987328.88940417/v1

67. Suárez-Ibarra, J. Y. *et al.* Time-spatial boundaries of bioecozonations (planktonic foraminifera) in the latest Quaternary: a case study from the western South Atlantic. *Rev. Micropaleontol.* **73**, (2021).

68. Suárez-Ibarra, J. Y., Frozza, C. F., Petró, S. M. & Pivel, M. A. G. Fragment or broken? Improving the planktonic foraminifera fragmentation assessment. *Palaios* **36**, 165–172 (2021).

69. Frozza, C. F., Pivel, M. A. G., Suárez-Ibarra, J. Y., Ritter, M. N. & Coimbra, J. C. Bioerosion on Late Quaternary Planktonic Foraminifera Related to Paleoproductivity in the Western South Atlantic. *Paleoceanogr. Paleoclimatology* **35**, 1–16 (2020).

70. Rodrigues, A. R., Pivel, M. A. G., Schmitt, P., Almeida, F. K. De & Bonetti, C. Marine Micropaleontology Infaunal and epifaunal benthic foraminifera species as proxies of organic matter paleo fl uxes in the Pelotas Basin , south-western Atlantic Ocean. *Mar. Micropaleontol.* **144**, 38–49 (2018).

71. Petró, S. M., Pivel, M. A. G. & Coimbra, J. C. Evidence of supra-lysoclinal dissolution of pelagic calcium carbonate in the late Quaternary in the western South Atlantic. *Mar. Micropaleontol.* **166**, (2021).

72. Blaauw, M. & Christeny, J. A. Flexible paleoclimate age-depth models using an autoregressive gamma process. *Bayesian Anal.* **6**, 457–474 (2011).

73. Team, R. C. R: A Language and Environment for Statistical Computing. (2021).

74. Team, Rs. RStudio: Integrated Development Environment for R. Boston (2020). doi:http://www.rstudio.com

75. Heaton, T. J. *et al.* Marine20 - The Marine Radiocarbon Age Calibration Curve (0-55,000 cal BP). *Radiocarbon* **62**, 779–820 (2020).

76. Nadal de Masi, M. A. Prehistoric hunter-gatherer mobility on the southern Brazilian coast: Santa Catarina Island. (Standford University, 1999).

77. Angulo, R. J., De Souza, M. C., Reimer, P. J. & Sasaoka, S. K. Reservoir effect of the southern and southeastern Brazilian coast. *Radiocarbon* **47**, 67–73 (2005).

78. Alves, E. *et al.* Radiocarbon reservoir corrections on the Brazilian coast from pre-bomb marine shells. *Quat. Geochronol.* **29**, 30–35 (2015).

79. Schiebel, R. & Hemleben, C. *Planktic Foraminifers in the Modern Ocean: Ecology, Biogeochemistry, and Application*. (2017). doi:10.1007/978-3-662-50297.6

80. Brummer, G. J. A. & Kučera, M. Taxonomic review of living planktonic foraminifera. *J. Micropalaeontology* **41**, 29–74 (2022).

81. Morard, R. *et al.* Genetic and morphological divergence in the warm-water planktonic foraminifera genus Globigerinoides. *PLoS One* **14**, 1–30 (2019).

82. Hutson, W. H. The Agulhas Current During the Late Pleistocene : Analysis of Modern Faunal Analogs. *Science (80-.).* **207**, 64–66 (1980).

83. Hammer, O., Harper, D. A. T. & Ryan, P. D. PAST: PALEONTOLOGICAL STATISTICS SOFTWARE PACKAGE FOR EDUCATION AND DATA ANALYSIS. *Palaeontol. Electron.* **4**, 1–9 (2001).

84. Siccha, M. & Kucera, M. ForCenS , a curated database of planktonic foraminifera census counts in marine surface sediment samples. *Sci. Data* **4**, 1–12 (2017).

85. García Chapori, N. & Laprida, C. Planktonic foraminifera assemblages from the Brazil–Malvinas Confluence: palaeoceanographic implications of sub-surface

temperature reconstructions in the western South Atlantic. *Lethaia* **54**, 477–494 (2021).

86. Locarnini, R. A. *et al.* World Ocean Atlas, Volume 1: Temperature. in *NOAA Atlas NESDIS* (ed. Mishonov, A.) 1–40 (2013).

87. Schlitzer, R. Ocean Data View. (2023). doi:https://odv.awi.de

88. Divakar Naidu, P. Distribution of upwelling index planktonic foraminifera in the sediments of the Western continental margin of India. *Oceanol. ACTA* **13**, 327–334 (1990).

89. Vénec-Peyré, M. T. & Caulet, J. P. Paleoproductivity changes in the upwelling system of Socotra (Somali Basin, NW Indian Ocean) during the last 72,000. years: Evidence from biological signatures. *Mar. Micropaleontol.* **40**, 321–344 (2000).

90. Wu, Y. *et al.* Assessing neodymium isotopes as an ocean circulation tracer in the Southwest Atlantic. *Earth Planet. Sci. Lett.* **599**, 117846 (2022).

91. Tachikawa, K. *et al.* The large-scale evolution of neodymium isotopic composition in the global modern and Holocene ocean revealed from seawater and archive data. *Chem. Geol.* **457**, 131–148 (2017).

92. Howe, J. N. W. *et al.* North Atlantic Deep Water Production during the Last Glacial Maximum. *Nat. Commun.* **7**, 1–8 (2016).

93. Pöppelmeier, F. *et al.* Neodymium isotopes as a paleo-water mass tracer: A model-data reassessment. *Quat. Sci. Rev.* **279**, (2022).

94. Robinson, S. *et al.* Simulating marine neodymium isotope distributions using Nd v1.0 coupled to the ocean component of the FAMOUS-MOSES1 climate model: sensitivities to reversible scavenging efficiency and benthic source distributions. *Geosci. Model Dev.* **16**, 1231–1264 (2023).

95. Gu, F. *et al.* Long-term vegetation , climate and ocean dynamics inferred from a 73 , 500 years old marine sediment core (GeoB2107-3) off southern. **172**, (2017).

96. Alvarenga, A. *et al.* S/SE Brazilian continental margin sea surface temperature and productivity changes over the last 50 kyr. *Palaeogeogr. Palaeoclimatol. Palaeoecol.* **601**, (2022).

97. Pedrão, G. A. *et al.* Marine Paleoproductivity From the Last Glacial Maximum to the Holocene in the Southwestern Atlantic: A Coccolithophore Assemblage and Geochemical Proxy Perspective. *Front. Earth Sci.* **10**, 1–16 (2022).

98. Mahiques, M. M. *et al.* Sedimentary changes on the Southeastern Brazilian upper slope during the last 35,000 years. *An. Acad. Bras. Cienc.* **79**, 171–181 (2007).

99. Lessa, D. V. O. *et al.* Holocene oscillations of Southwest Atlantic shelf circulation based on planktonic foraminifera from an upwelling system (off Cabo Frio , Southeastern Brazil). (2016). doi:10.1177/0959683616638433

100. Ferreira, F., Frontalini, F., Leao, C. & Leipnitz, I. Changes in the water column structure and paleoproductivity in the western South Atlantic Ocean since the middle Pleistocene : Evidence from benthic and planktonic foraminifera. *Quat. Int.* **352**, 111–123 (2014).

101. Souto, D. D. *et al.* Marine sediments from southeastern Brazilian continental shelf: A 1200 year record of upwelling productivity. *Palaeogeogr. Palaeoclimatol. Palaeoecol.* **299**, 49–55 (2011).

102. Venancio, I. M. *et al.* Influence of continental shelf processes in the water mass balance and productivity from stable isotope data on the Southeastern Brazilian coast. *J. Mar. Syst.* **139**, 241–247 (2014).

103. Venancio, I. M., Gomes, V. P., Belem, A. L. & Albuquerque, A. L. S. Surface-to-subsurface temperature variations during the last century in a western boundary upwelling system (Southeastern, Brazil). *Cont. Shelf Res.* **125**, 97–106 (2016).

104. Leonhardt, A., Toledo, F. A. L. & Coimbra, J. C. The productivity history in the Southwestern Atlantic as inferred from coccolithophore record for the last 130 kyr. *Rev. Bras. Paleontol.* **16**, (2013).

105. Lessa, D. V. O., Santos, T. P., Venancio, I. M. & Albuquerque, A. L. S. Offshore expansion of the Brazilian coastal upwelling zones during Marine Isotope Stage 5. *Glob. Planet. Change* **158**, 13–20 (2017).

106. Gonçalves, J. D. F. & Leonhardt, A. Mechanisms of fertilization inferred from the coccolithophorid record during the Late Quaternary in the southern Brazilian Continental Margin. *Rev. Bras. Paleontol.* **25**, 76–89 (2022).

107. Conan, S. M. & Brummer, G. A. Fluxes of planktic foraminifera in response to monsoonal upwelling on the Somalia Basin margin. *Deep. Res. Part II* **47**, 2207–2227 (2000).

108. Toledo, F. A. L., Costa, K. B., Pivel, M. A. G. & Campos, E. J. D. TRACING PAST CIRCULATION CHANGES IN THE WESTERN SOUTH ATLANTIC BASED ON PLANKTONIC FORAMINIFERA. *Rev. Bras. Paleontol.* **11**, 169–178 (2008).

109. Lessa, D. V. *et al.* Planktonic foraminifera in the sediment of a western boundary upwelling system off Cabo Frio, Brazil. *Mar. Micropaleontol.* **106**, 55–68 (2014).

110. Sousa, S. H. M., Godoi, S. S. De, Amaral, P. G. C., Vicente, T. M. & Martins, M. V. A. Distribution of living planktonic foraminifera in relation to oceanic processes on the southeastern continental Brazilian. *Cont. Shelf Res.* **89**, 76–87 (2014).

111. Bahr, A. *et al.* A Comparison Study of Mg/Ca-, Alkenone-, and TEX86-Derived Temperatures for the Brazilian Margin. *Paleoceanogr. Paleoclimatology* **38**, 1–17 (2023).

112. Iwai, F. S., Bianchi, M., Costa, K. B. & Toledo, F. A. L. Planktonic foraminifera abundances of core KF-I [DATASET]. *PANGAEA* (2018). doi:10.1594/PANGAEA.893111

113. Iwai, F. S., Bianchi, M., Costa, K. B. & Toledo, F. A. L. Planktonic foraminifera abundances of core KF-H [DATASET]. *PANGAEA* (2018).

114. Duque-Castaño, M., Leonhardt, A. & Pivel, M. A. G. Planktonic Foraminifera

assemblages from sediment core SIS-188 [DATASET]. *PANGAEA* (2024).

115. Zweng, M. . *et al.* World Ocean Atlas, Volume 2: Salinity. in *NOAA Atlas NESDIS 82* (ed. Mishonov, A.) 1–39 (2013).

116. Lisiecki, L. E. & Stern, J. V. Regional and global benthic d18O stacks for the last glacial cycle. *Paleoceanography* **31**, 1368–1394 (2016).

117. Duque-Castaño, M., Leonhardt, A. & Pivel, M. A. G. Morphometric analysis in the shells of the planktonic foraminifera Orbulina universa: a source for paleoceanographic information? *Brazilian J. Oceanogr.* **67**, 1–17 (2019).

118. Luz, L. G. *et al.* Contrasting late-glacial paleoceanographic evolution between the upper and lower continental slope of the western South Atlantic Contrasting late-glacial paleoceanographic evolution between the upper and lower continental slope of the western South Atlant. (2020). doi:10.5194/cp-16-1245-2020

119. Weschenfelder, J., Baitelli, R., Corrêa, I. C. S., Bortolin, E. C. & dos Santos, C. B. Quaternary incised valleys in southern Brazil coastal zone. *J. South Am. Earth Sci.* **55**, 83–93 (2014).

120. Lantzsch, H., Hanebuth, T. J. J., Chiessi, C. M., Schwenk, T. & Violante, R. A. The high-supply , current-dominated continental margin of southeastern South America during the late Quaternary. *Quat. Res.* **81**, 339–354 (2014).

121. Nagai, R. H., Sousa, S. H. de M. e, Lourenco, R. A., Bicego, M. C. & Mahiques, M. M. de. Paleoproductivity Changes During the Late Quaternary in the Southeastern. *Brazilian J. Oceanogr.* **58**, 31–41 (2010).

122. Bickert, T. & Wefer, G. Late Quaternary deep water circulation in the South Atlantic: Reconstruction from carbonate dissolution and benthic stable isotopes. in *The South Atlantic: Present and Past Circulation* (eds. Wefer, G., Berger, W. H., Siedler, G. & Webb, D.) 599–620 (Springer-Verlag, 1996).

123. Laskar, J. *et al.* A long term numerical solution for the insolation quantities of the Earth. *Astron. Astrophys.* **428**, 261–285 (2004).

124. Kohfeld, K. E. & Chase, Z. Temporal evolution of mechanisms controlling ocean carbon uptake during the last glacial cycle. *Earth Planet. Sci. Lett.* **472**, 206–215 (2017).

125. Gardner, J. V. Late Pleistocene carbonate dissolution cycles in the eastern equatorial Atlantic. in *Dissolution of deep-sea carbonates1* (eds. Sliter, W. V, Be, A. W. H. & Berger, W. H.) 129–141 (Cushman Foundation for Foraminfieral Research, 1975).

126. Wolff, E. W. *et al.* Southern Ocean sea-ice extent, productivity and iron flux over the past eight glacial cycles. *Nature* **440**, 491–496 (2006).

127. Mejía, L. M. *et al.* Effects of midlatitude westerlies on the paleoproductivity at the Agulhas Bank slope during the penultimate glacial cycle: Evidence from coccolith Sr/Ca ratios. *Paleoceanography* **29**, 697–714 (2014).

128. Dezileau, L. *et al.* Iron control of past productivity in the coastal upwelling system off the Atacama Desert, Chile. *Paleoceanography* **19**, (2004).

129. Buesseler, K. O. & Andrews, J. E. The Effects of Iron Fertilization. *Science (80-.).* **304**, 414–417 (2004).

130. Roth, R., Ritz, S. P. & Joos, F. Burial-nutrient feedbacks amplify the sensitivity of atmospheric carbon dioxide to changes in organic matter remineralisation. *Earth Syst. Dyn.* **5**, 321–343 (2014).

131. Kohfeld, K. E. *et al.* Southern Hemisphere westerly wind changes during the Last Glacial Maximum : paleo-data synthesis. *Quat. Sci. Rev.* **68**, 76–95 (2013).

132. Martin, J. H. Glacial-interglaccial CO2 change: the iron hypothesis. *Paleoceanography* **5**, 1–13 (1990).

133. Boscolo-Galazzo, F., Crichton, K. A., Barker, S. & Pearson, P. N. Temperature dependency of metabolic rates in the upper ocean: A positive feedback to global climate change? *Glob. Planet. Change* **170**, 201–212 (2018).

134. Rutberg, R. L., Hemming, S. R. & Goldstein, S. L. Reduced North Atlantic Deep Water flux to the glacial Southern Ocean inferred from neodymium isotope ratios. *Nature* **405**, 935–938 (2000).

135. Jonkers, L. *et al.* Deep circulation changes in the central South Atlantic during the past 145 kyrs reflected in a combined231Pa/230Th, Neodymium isotope and benthic δC13 record. *Earth Planet. Sci. Lett.* **419**, 14–21 (2015).

136. Marzocchi, A. & Jansen, M. F. Global cooling linked to increased glacial carbon storage via changes in Antarctic sea ice. *Nat. Geosci.* **12**, 1001–1005 (2019).

137. Chalk, T. B., Foster, G. L. & Wilson, P. A. Dynamic storage of glacial CO 2 in the Atlantic Ocean revealed by boron [CO 32−] and pH records. *Earth Planet. Sci. Lett.* **510**, 1–11 (2019).

138. Yu, J. *et al.* Last glacial atmospheric CO2 decline due to widespread Pacific deep-water expansion. *Nat. Geosci.* **13**, 628–633 (2020).

139. Bard, E. & Rickaby, R. E. M. Migration of the subtropical front as a modulator of glacial climate. *Nature* **460**, 380–383 (2009).

140. Ballalai, J. M. *et al.* Tracking spread of the Agulhas Leakage into the western South Atlantic and its northward transmission during the Last Interglacial. *Paleoceanogr. Paleoclimatology* **34**, 1–17 (2019).

141. MacAyeal, D. R. A catastrophe model of the paleoclimate. *J. Glaciol.* **24**, 245–257 (1979).

142. Tzedakis, P. C., Crucifix, M., Mitsui, T. & Wolff, E. W. A simple rule to determine which insolation cycles lead to interglacials. *Nature* **542**, 427–432 (2017).

143. EPICA. Eight glacial cycles from an Antarctic ice core. *Nature* **429**, 623–628 (2004).

144. Hoegh-Guldberg, O. & Bruno, J. F. The impact of climate change on the world's marine ecosystems. *Science (80-.).* **328**, 1523–1528 (2010).

145. Roy, T., Lombard, F., Bopp, L. & Gehlen, M. Projected impacts of climate change and ocean acidification on the global biogeography of planktonic Foraminifera. *Biogeosciences* **12**, 2873–2889 (2015).

146. Przeslawski, R., Falkner, I., Ashcroft, M. B. & Hutchings, P. Using rigorous selection criteria to investigate marine range shifts. *Estuar. Coast. Shelf Sci.* **113**, 205–212 (2012).

147. Beaugrand, G., Mcquatters-Gollop, A., Edwards, M. & Goberville, E. Long-term responses of North Atlantic calcifying plankton to climate change. *Nat. Clim. Chang.* **3**, 263–267 (2013).

148. Riebesell, U. *et al.* Reduced calcification of marine plankton in response to increased atmospheric CO2. *Nature* **407**, 364–366 (2000).

149. Lombard, F., Da Rocha, R. E., Bijma, J. & Gattuso, J. P. Effect of carbonate ion concentration and irradiance on calcification in planktonic foraminifera. *Biogeosciences* **7**, 247–255 (2010).

150. Manno, C., Morata, N. & Bellerby, R. Effect of ocean acidification and temperature increase on the planktonic foraminifer Neogloboquadrina pachyderma (sinistral). *Polar Biol.* **35**, 1311–1319 (2012).

151. Kawahata, H. *et al. Perspective on the response of marine calcifiers to global warming and ocean acidification—Behavior of corals and foraminifera in a high CO2 world "hot house". Progress in Earth and Planetary Science* **6**, (Progress in Earth and Planetary Science, 2019).

152. Iwasaki, S., Kimoto, K., Sasaki, O., Kano, H. & Uchida, H. Sensitivity of planktic foraminiferal test bulk density to ocean acidification. *Sci. Rep.* **9**, 1–9 (2019).

153. Davis, C. V. *et al.* Ocean acidification compromises a planktic calcifier with implications for global carbon cycling. *Sci. Rep.* **7**, 1–8 (2017).

154. De Moel, H. *et al.* Planktic foraminiferal shell thinning in the arabian sea due to anthropogenic ocean acidification? *Biogeosciences* **6**, 1917–1925 (2009).

155. Field, D., Baugmgartner, T., Charles, C., Ferreira-Bartrina, V. & Ohman, M. Planktonic foraminifera of the California Current reflect 20th-Century Warming. *Science (80-.).* **311**, 63–66 (2006).

156. Jonkers, L., Hillebrand, H. & Kucera, M. Global change drives modern plankton communities away from the pre-industrial state. *Nature* **570**, 372–375 (2019).

157. Fox, L., Stukins, S., Hill, T. & Miller, C. G. Quantifying the Effect of Anthropogenic Climate Change on Calcifying Plankton. *Sci. Rep.* **10**, 1–9 (2020).

158. Schmidt, D. N., Renaud, S., Bollmann, J., Schiebel, R. & Thierstein, H. R. Size distribution of Holocene planktic foraminifer assemblages: Biogeography, ecology and adaptation. *Mar. Micropaleontol.* **50**, 319–338 (2004).

159. Ortiz, J. D., Mix, A. C. & Collier, R. W. Environmental control of living symbiotic and asymbiotic foraminifera of the California Current. *Paleoceanography* **10**, 987–1009 (1995).

160. Berger, W. H. Foraminiferal ooze: Solution at depths. *Science (80-.).* **156**, 383–385 (1967).

161. Berger, W. H. Planktonic foraminifera: selective solution and the lysocline. *Mar. Geol.* **8**, 111–138 (1970).

162. Bé, A. W. H., Morse, J. W. & Harrison, S. M. Progressive dissolution and ultrastructural breakdown of planktonic foraminifera. in *Dissolution of deep-sea carbonates* (eds. Sliter, W. V, Bé, A. W. H. & Berger, W. H.) 27–55 (Cushman Foundation for Foraminfieral Research, 1975).

163. Monnin, E. *et al.* Atmospheric CO2 concentrations over the last glacial termination. *Science (80-.).* **291**, 112–114 (2001).

164. Broecker, W. Ocean chemistry during glacial time. *Geochim. Cosmochim. Acta* **46**, 1689–1705 (1982).

165. Shackleton, N. J. The 100 , 000-Year Ice-Age Cycle Identified and Found to Lag

Temperature , Carbon Dioxide , and Orbital Eccentricity. **289**, 1897–1902 (2000).

166. Lenton, T. M. *et al.* Tipping elements in the Earth's climate system. *Proc. Natl. Acad. Sci. U. S. A.* **105**, 1786–1793 (2008).

167. Railsback, L. B., Gibbard, P. L., Head, M. J., Voarintsoa, N. R. G. & Toucanne, S. An optimized scheme of lettered marine isotope substages for the last 1.0 million years, and the climatostratigraphic nature of isotope stages and substages. *Quat. Sci. Rev.* **111**, 94–106 (2015).

168. Rickaby, R. E. M., Elderfield, H., Roberts, N., Hillenbrand, C. D. & Mackensen, A. Evidence for elevated alkalinity in the glacial Southern Ocean. *Paleoceanography* **25**, 1–15 (2010).

169. Clark, P. U. *et al.* The Last Glacial Maximum. *Science (80-.).* **325**, 710–714 (2009).

170. Petró, S. M. & Burone, L. CHANGES IN WATER MASSES IN THE LATE Q UATERNARY RECORDED AT URUGUAYAN CONTINENTAL SLOPE (SOUTH A TLANTIC OCEAN). *J. Sediment. Environ.* **3**, 280–289 (2018).

171. Petró, S. M., Pivel, M. A. G. & Coimbra, J. C. Evidence of supra-lysoclinal dissolution of pelagic calcium carbonate in the late Quaternary in the western South Atlantic. *Mar. Micropaleontol.* **166**, (2021).

172. Petró, S. M., Oliveira, E. da C., Alejandra, M. P. G. & Coimbra, J. C. Registro das Flutuações da Lisoclina e da CCD no Quaternário Tardio na Bacia de Pelotas. *Anuário do Inst. Geociências - UFRJ* **41**, 710–719 (2018).

173. Broecker, W. The Great Ocean Conveyor. *Oceanography* **4**, 79–89 (1991).

174. Howe, J. N. W. *et al.* Similar mid-depth Atlantic water mass provenance during the Last Glacial Maximum and Heinrich Stadial 1. *Earth Planet. Sci. Lett.* **490**, 51–61 (2018).

175. Howe, J. N. W. *et al.* Antarctic intermediate water circulation in the South Atlantic

over the past 25,000 years. *Paleoceanography* **31**, 1302–1314 (2016).

176. Jeandel, C. Concentration and isotopic composition of Nd in the South Atlantic Ocean. *Earth Planet. Sci. Lett.* **117**, 581–591 (1993).

177. Garcia, H. E. *et al.* World Ocean Atlas, Volume 4: Dissolved Inorganic Nutrients (phosphate, nitrate, silicate). in *NOAA Atlas NESDIS* (ed. Mishonov, A.) 1–25 (2014).

178. Skinner, L. C. *et al.* North atlantic versus southern ocean contributions to a deglacial surge in deep ocean ventilation. *Geology* **41**, 667–670 (2013).

179. Conan, S. M. H., Ivanova, E. M. & Brummer, G. J. A. Quantifying carbonate dissolution and calibration of foraminiferal dissolution indices in the Somali Basin. *Mar. Geol.* **182**, 325–349 (2002).

180. Parker, F. L. & Berger, W. H. Faunal and solution patterns of planktonic foraminifera in surface sediments of the South Pacific. *Deep. Res. Part I* **18**, 73–107 (1971).

181. Kucera, M. Planktonic Foraminifera as tracers of past oceanic environments. in *Proxies in Late Cenozoic Paleoceanography* (ed. Hillaire-Marcel, C.) 213–254 (Elsevier, 2007).

182. Berger, W. H. Planktonic Foraminifera: Selective solution and the lysocline. *Mar. Geol.* **8**, 111–138 (1970).

183. Le, J. & Shackleton, N. J. Carbonate dissolution fluctuations in the western equatorial pacific during the late quaternary. *Paleoceanography* **7**, 21–42 (1992).

184. Berger, W. H., Bonneau, M. C. & Parker, F. L. Foraminifera on the deep-sea floor : lysocline and dissolution rate. *Oceanol. ACTA* **5**, 249–258 (1982).

185. Steinsund, P. I. & Hald, M. Recent calcium carbonate dissolution in the Barents Sea: Paleoceanographic applications. *Mar. Geol.* **117**, 303–316 (1994).

186. Nguyen, T. M. P. & Speijer, R. P. A new procedure to assess dissolution based on

experiments on Pliocene-Quaternary foraminifera (ODP Leg 160, Eratosthenes Seamount, Eastern Mediterranean). *Mar. Micropaleontol.* **106**, 22–39 (2014).

187. Gonzales, M. V *et al.* Help index : Hoeglundina elegans preservation index for marine sediments in the western South Atlantic. *J. Foraminifer. Res.* **47**, 59–69 (2017).

188. McCave, I. N., Manighetti, B. & Robinson, S. G. Sortable silt and fine sediment size/composition: Parameters for Palaeocurrent Speed and Palaeoceanography. *Paleoceanography* **10**, 593–610 (1995).

189. McCave, I. N. & Hall, I. R. Size sorting in marine muds: Processes, pitfalls, and prospects for paleoflow-speed proxies. *Geochemistry, Geophys. Geosystems* **7**, (2006).

190. McCave, I. N. & Andrews, J. T. Distinguishing current effects in sediments delivered to the ocean by ice. I. Principles, methods and examples. *Quat. Sci. Rev.* **212**, 92–107 (2019).

191. Santos, T. P. *et al.* Stable oxygen isotope record during Termination II in sediment core GL1090. *PANGAEA* (2017). doi:10.1594/PANGAEA.884583

192. Marchitto, T. M. *et al.* Improved oxygen isotope temperature calibrations for cosmopolitan benthic foraminifera. *Geochim. Cosmochim. Acta* **130**, 1–11 (2014).

193. Zahn, R., Winn, K. & Sarnthein, M. Benthic foraminiferal δ13C and accumulation rates of organic carbon Uvigerina peregrina group and Cibicidoides wuellerstorfi. *Paleoceanography* **1**, 27–42 (1986).

194. Dias, B. B. *et al.* Coupled changes in western South Atlantic carbon sequestration and particle reactive element cycling during millennial-scale Holocene climate variability. *Sci. Rep.* **11**, 1–12 (2021).

195. Tanaka, T. *et al.* JNdi-1: A neodymium isotopic reference in consistency with LaJolla neodymium. *Chem. Geol.* **168**, 279–281 (2000).

196. Jollife, I. T. & Cadima, J. Principal component analysis: A review and recent developments. *Philos. Trans. R. Soc. A Math. Phys. Eng. Sci.* **374**, (2016).

197. Hua, Q. Radiocarbon: A chronological tool for the recent past. *Quat. Geochronol.* **4**, 378–390 (2009).

198. Anderson, E. C. *et al.* Natural radiocarbon from cosmic radiation. *Phys. Rev.* **72**, 931–936 (1947).

199. Paillard, D., Labeyrie, L. & Yiou, P. Macintosh Program performs time-series analysis. *Eos, Trans. Am. Geophys. Union* **77**, 379–379 (1996).

200. Gu, F., Chiessi, C. M., Zonneveld, K. A. F. & Behling, H. Late Quaternary environmental dynamics inferred from marine sediment core GeoB6211-2 o ff southern Brazil. *Palaeogeogr. Palaeoclimatol. Palaeoecol.* **496**, 48–61 (2018).

201. Takahashi, K. & Be, A. W. H. Planktonic foraminifera: factors controlling sinking speeds. *Deep Sea Res. Part A, Oceanogr. Res. Pap.* **31**, 1477–1500 (1984).

202. Schiebel, R. *Planktic Foraminifers in the Modern Ocean*.

203. Bach, L. T. *et al.* The Influence of Plankton Community Structure on Sinking Velocity and Remineralization Rate of Marine Aggregates. *Global Biogeochem. Cycles* **33**, 971–994 (2019).

204. Berelson, W. M. *et al.* Relating estimates of CaCO3 production, export, and dissolution in the water column to measurements of CaCO3 rain into sediment traps and dissolution on the sea floor:A revised global carbonate budget. *Global Biogeochem. Cycles* **21**, 1–15 (2007).

205. Mcmanus, J. F., Francois, R., Gherardi, J. & Keigwin, L. D. Collapse and rapid resumption of Atlantic meridional circulation linked to deglacial climate changes. **428**, 1–4 (2004).

206. Lippold, J. *et al.* Does sedimentary 231Pa/230Th from the Bermuda Rise monitor past Atlantic Meridional Overturning Circulation ? *Geophys. Res. Lett.* **36**, 1–6

(2009).

207. de Boer, B. ., Lourens, L. J. . & van de Wal, R. S. W. Global 5 Million Year Sea Level, Temperature, and d18Osw Reconstructions. [Eustatic sea level]. *NOAA/WDS Paleoclimatology - NOAA Natl. Centers Environ. Information.* (2015). doi:doi.org/10.25921/xs31-nt56

208. Oppo, D. W. *et al.* Deglacial Temperature and Carbonate Saturation State Variability in the Tropical Atlantic at Antarctic Intermediate Water Depths. *Paleoceanogr. Paleoclimatology* **38**, (2023).

209. Curry, W. B., Duplessy, J. C., Labeyrie, L. D. & Shackleton, N. J. CHANGES IN THE DISTRIBUTION OF δ13C OF DEEP WATER ΣCO2 BETWEEN THE LAST GLACIATION AND THE HOLOCENE. *Paleoceanography* **3**, 317–341 (1988).

210. Duplessy, J. *et al.* 13C Record of Benthic Foraminifera in the Last Interglacial Ocean : Implications for the Carbon Cycle and the Global Deep Water Circulation. **243**, 225–243 (1984).

211. Curry, W. B. & Oppo, D. W. Glacial water mass geometry and the distribution of d13C of ΣCO2 in the western Atlantic Ocean. *Paleoceanography* **20**, 1–13 (2005).

212. Duplessy, J. C. *et al.* Deepwater source variations during the last climatic cycle and their impact on the global deepwater circulation. *Paleoceanography* **3**, 343–360 (1988).

213. Mackensen, A. On the use of benthic foraminiferal δ13C in palaeoceanography : constraints from primary proxy relationships. *Geol. Soc. London, Spec. Publ.* **303**, 121–133 (2008).

214. Hesse, T., Lohmann, G., Bijma, J., Mackensen, A. & Zeebe, R. E. Modelling d13C in benthic foraminifera: insights from model sensitivity experiments. *Mar. Micropaleontol.* **112**, 50–61 (2014).

215. Key, R. M. *et al.* A global ocean carbon climatology: Results from Global Data

Analysis Project (GLODAP). *Global Biogeochem. Cycles* **18**, 1–23 (2004).

216. Portilho-Ramos, R. C. *et al.* Methane release from the southern Brazilian margin during the last glacial. *Sci. Rep.* **8**, (2018).

217. Santos, T. P. *et al.* Prolonged warming of the Brazil Current precedes deglaciations Prolonged warming of the Brazil Current precedes deglaciations. *Earth Planet. Sci. Lett.* **463**, 1–12 (2017).

218. Gottschalk, J. *et al.* Carbon isotope offsets between benthic foraminifer species of the genus Cibicides (Cibicidoides) in the glacial sub-Antarctic Atlantic. *Paleoceanography* **31**, 1583–1602 (2016).

219. Piepgraas, D. J. & Wasserburg, G. J. Neodymium isotopic variations in seawater. *Earth Planet. Sci. Lett.* **50**, 128–138 (1980).

220. Frank, M. Radiogenic isotopes: Tracers of past ocean circulation and erosional input. *Rev. Geophys.* **40**, 1-1-1–38 (2002).

221. Piotrowski, A. M., Goldstein, S. L., Hemming, S. R., Fairbanks, R. G. & Zylberberg, D. R. Oscillating glacial northern and southern deep water formation from combined neodymium and carbon isotopes. *Earth Planet. Sci. Lett.* **272**, 394–405 (2008).

222. Blaser, P. *et al.* The resilience and sensitivity of Northeast Atlantic deep water εNd to overprinting by detrital fluxes over the past 30,000 years. *Geochim. Cosmochim. Acta* **245**, 79–97 (2019).

223. Karas, C., Goldstein, S. L. & deMenocal, P. B. Evolution of Antarctic Intermediate Water during the Plio-Pleistocene and implications for global climate: Evidence from the South Atlantic. *Quat. Sci. Rev.* **223**, 1–11 (2019).

224. Pöppelmeier, F. *et al.* Stable Atlantic Deep Water Mass Sourcing on Glacial-Interglacial Timescales. *Geophys. Res. Lett.* **48**, 1–10 (2021).

225. Pöppelmeier, F. *et al.* Water mass gradients of the mid-depth Southwest Atlantic

during the past 25,000 years. *Earth Planet. Sci. Lett.* **531**, (2020).

226. Pérez-Asensio, J. N. *et al.* Glacial expansion of carbon-rich deep waters into the Southwestern Indian Ocean over the last 630 kyr. *Glob. Planet. Change* **230**, (2023).

227. Kerr, J., Rickaby, R. E. M., Yu, J., Elderfield, H. & Sadekov, A. Y. The effect of ocean alkalinity and carbon transfer on deep-sea carbonate ion concentration during the past five glacial cycles. *Earth Planet. Sci. Lett.* **471**, 42–53 (2017).